Ill posedness in modelling two-dimensional morphodynamic problems
Effects of bed slope and secondary flow

Chavarrías, Víctor; Schielen, Ralph; Ottevanger, Willem; Blom, Astrid

DOI
10.1017/jfm.2019.166

Publication date
2019

Document Version
Accepted author manuscript

Published in
Journal of Fluid Mechanics

Citation (APA)
Chavarrías, V., Schielen, R., Ottevanger, W., & Blom, A. (2019). Ill posedness in modelling two-dimensional morphodynamic problems: Effects of bed slope and secondary flow. *Journal of Fluid Mechanics*, *868*, 461-500. https://doi.org/10.1017/jfm.2019.166

Ill-posedness in modelling 2D morphodynamic problems: Effects of bed slope and secondary flow

Víctor Chavarrías *[1], Ralph Schielen[2,3], Willem Ottevanger[4], and Astrid Blom[1]

[1]Faculty of Civil Engineering and Geosciences, Delft University of Technology, Delft, The Netherlands.

[2]Faculty of Engineering Technology, University of Twente, Enschede, The Netherlands.

[3]Ministry of Infrastructure and Water Management-DG Rijkswaterstaat, Lelystad, The Netherlands.

[4]Deltares, Delft, The Netherlands.

14th February, 2019

Abstract

A two-dimensional model describing river morphodynamic processes under mixed-size sediment conditions is analysed with respect to its well-posedness. Well-posedness guarantees the existence of a unique solution continuously depending on the problem data. When a model becomes ill-posed, infinitesimal perturbations to a solution grow infinitely fast. Apart from the fact that this behaviour cannot represent a physical process, numerical simulations of an ill-posed model continue to change as the grid is refined. For this reason, ill-posed models cannot be used as predictive tools. One source of ill-posedness is due to the simplified description of the processes related to vertical mixing of sediment. The current analysis reveals the existence of two additional mechanisms that lead to model ill-posedness: secondary flow due to the flow curvature and the gravitational pull on the sediment transport direction. When parametrising secondary flow, accounting for diffusion in the transport of secondary flow intensity is a requirement for obtaining a well-posed model. When considering the theoretical amount of diffusion, the model predicts instability of perturbations that are incompatible with the shallow water assumption. The gravitational pull is a necessary mechanism to yield a well-posed model, but not all closure relations to account for this mechanism are valid under mixed-size sediment conditions. Numerical simulations of idealised situations confirm the results of the stability analysis and highlight the consequences of ill-posedness.

*Corresponding author: v.chavarriasborras@tudelft.nl

1 Introduction

Modelling of fluvial morphodynamic processes is a powerful tool not only to predict the future state of a river after, for instance, an intervention or a change in the discharge regime (*Blom et al.*, 2017), but also as a source of understanding of the natural processes responsible for patterns such as dunes, meanders, and bars (*Callander*, 1969; *Seminara*, 2006; *Colombini and Stocchino*, 2012). A framework for modelling the morphodynamic development of alluvial rivers is composed of a system of partial differential equations for modelling the flow, change in bed elevation, and change in the bed surface texture. The *Saint-Venant* (1871) equations account for conservation of water mass and momentum and enable modelling processes with a characteristic length scale significantly longer than the flow depth in one-dimensional cases. The Shallow Water Equations describe the depth-averaged flow in two-dimensional cases. Conservation of unisize bed sediment is typically modelled using the *Exner* (1920) equation and, under mixed-size sediment conditions, the active layer model (*Hirano*, 1971) accounts for mass conservation of bed sediment of each grain size.

Although widely successful in predicting river morphodynamics, a fundamental problem arises when using the above framework. Under certain conditions the description of the natural phenomena is not captured by the system of equations, which manifests as an ill-posed model. Models describe a simplified version of reality, which allows us to understand the key elements playing a major role in the dynamics of the system one studies (*Paola and Leeder*, 2011). Major simplifications such as reducing streamwise morphodynamic processes to a diffusion equation allow for insight on the creation of stratigraphic records and evolution on large spatial scales (*Paola et al.*, 1992; *Paola*, 2000; *Paola and Leeder*, 2011). There is a difference between greatly simplified models and models that do not capture the physical processes. A simplified model reproduces a reduced-complexity version of reality (*Murray*, 2007) and it is mathematically well-posed, as a unique solution exists that depends continuously on the data (*Hadamard*, 1923; *Joseph and Saut*, 1990). An ill-posed model lacks crucial physical processes that cause the model to be unsuitable to capture the dynamics of the system (*Fowler*, 1997). An ill-posed model is unrepresentative of a physical phenomenon, as the growth rate of infinitesimal perturbations to a solution (i.e., negligible noise from a physical perspective) tends to infinity (*Kabanikhin*, 2008). This is different from chaotic systems, in which noise similarly causes the solution to diverge but not infinitely fast (*Devaney*, 1989; *Banks et al.*, 1992).

An example of an ill-posed model is the one describing the dynamics of granular flow. The continuum formulation of such a problem depends on deriving a model for the granular viscosity. *Jop et al.* (2005, 2006) relate viscosity to a dimensionless shear rate. The model captures the dynamics of granular flows if the dimensionless shear rate is within a certain range, but otherwise the model is ill-posed and loses its predictive capabilities (*Barker et al.*, 2015). A better representation of the physical processes guaranteeing that viscosity tends to 0 when the dimensionless shear rate tends

to 0 extends the domain of well-posedness (*Barker and Gray*, 2017).

Under unisize sediment and one-dimensional flow conditions, the Saint-Venant-Exner model may be ill-posed when the Froude number is larger than 6 (*Cordier et al.*, 2011). As most flows of interest are well below this limit, we can consider modelling of fluvial problems under unisize sediment conditions to be well-posed. This is not the case when considering mixed-size sediment. Using the active layer model we assume that the bed can be discretised into two layers: the active layer and the substrate. The sediment transport rate depends on the grain size distribution of the active layer. A vertical flux of sediment occurs between the active layer and the substrate if the elevation of the interface between the active layer and the substrate changes. The active layer is well-mixed, whereas the substrate can be stratified. The above simplification of the physical processes responsible for vertical mixing causes the active layer model to be ill-posed (*Ribberink*, 1987; *Stecca et al.*, 2014; *Chavarrías et al.*, 2018). In particular, the active layer is prone to be ill-posed under degradational conditions into a substrate finer than the active layer (i.e., an armoured bed (*Parker and Sutherland*, 1990)) for any value of the Froude number.

Previous analyses of river morphodynamic models regarding their well-posedness have been focused on conditions of one-dimensional flow (*Ribberink*, 1987; *Cordier et al.*, 2011; *Stecca et al.*, 2014; *Chavarrías et al.*, 2018). Our objective is to extend these analyses to conditions of two-dimensional flow. More specifically we include the secondary flow and the bed slope effect in the analysis of the well-posedness of the system of equations.

As the flow is intrinsically three-dimensional, the depth-averaging procedure eliminates an important flow component: the secondary flow (*Van Bendegom*, 1947; *Rozovskii*, 1957). The secondary flow causes, for instance, an increase in the amplitude of meanders (*Kitanidis and Kennedy*, 1984) and plays an important role in bar development (*Olesen*, 1982). To understand the morphology of two-dimensional features, it is necessary to account for the fact that the sediment transport direction is affected by the gravitational pull when the bed slope in the transverse direction is significant (*Dietrich and Smith*, 1984; *Seminara*, 2006). This is usually done using a closure relation that sets the angle between the flow and the sediment transport directions as a function of the flow and sediment parameters (*Van Bendegom*, 1947; *Engelund*, 1974; *Talmon et al.*, 1995; *Seminara et al.*, 2002; *Parker et al.*, 2003; *Francalanci and Solari*, 2007, 2008; *Baar et al.*, 2018).

In this paper we show that combining these two effects, secondary flow and sediment deflection by the bed slope, leads in some cases to an ill-posed system of equations. The paper is organised as follows. In Section 2 we present the model equations describing the primary and secondary flow, as well as changes in bed elevation and surface texture. In Section 3 we extend the explanation of ill-posedness and relate it to growth of perturbations. We subsequently conduct a stability analysis of the equations, which indicates the conditions under which the secondary flow model and the closure relation for the bed slope effect yield an ill-posed model (Section 4). In Section 5 we run

numerical simulations of idealised cases to test the validity of the analytical results and study the consequences of ill-posedness.

2 Mathematical Model

In this section we present the two-dimensional mathematical model of flow, accounting for secondary flow, coupled to a morphodynamic model for mixed-size sediment. We subsequently introduce the equations describing the primary flow (Section 2.1), the secondary flow (Section 2.2), and morphodynamic change (Section 2.3). In Section 2.4 we linearise the system of equations to study the stability of perturbations.

2.1 Primary Flow Equations

The primary flow is described using the depth-averaged Shallow Water Equations (e.g. *Vreugdenhil*, 1994):

$$\frac{\partial h}{\partial t} + \frac{\partial q_\mathrm{x}}{\partial x} + \frac{\partial q_\mathrm{y}}{\partial y} = 0 \,, \tag{1}$$

$$\begin{aligned} &\frac{\partial q_\mathrm{x}}{\partial t} + \frac{\partial (q_\mathrm{x}^2/h + gh^2/2)}{\partial x} + \frac{\partial \left(\frac{q_\mathrm{x} q_\mathrm{y}}{h}\right)}{\partial y} + gh\frac{\partial \eta}{\partial x} - F_\mathrm{sx} = \\ &= 2\frac{\partial}{\partial x}\left(\nu h \frac{\partial (\frac{q_\mathrm{x}}{h})}{\partial x}\right) + \frac{\partial}{\partial y}\left(\nu h \left(\frac{\partial (\frac{q_\mathrm{x}}{h})}{\partial y} + \frac{\partial (\frac{q_\mathrm{y}}{h})}{\partial x}\right)\right) - ghS_\mathrm{fx} \,, \end{aligned} \tag{2}$$

$$\begin{aligned} &\frac{\partial q_\mathrm{y}}{\partial t} + \frac{\partial (q_\mathrm{y}^2/h + gh^2/2)}{\partial y} + \frac{\partial \left(\frac{q_\mathrm{x} q_\mathrm{y}}{h}\right)}{\partial x} + gh\frac{\partial \eta}{\partial y} - F_\mathrm{sy} = \\ &2\frac{\partial}{\partial y}\left(\nu h \frac{\partial (\frac{q_\mathrm{y}}{h})}{\partial y}\right) + \frac{\partial}{\partial x}\left(\nu h \left(\frac{\partial (\frac{q_\mathrm{y}}{h})}{\partial x} + \frac{\partial (\frac{q_\mathrm{x}}{h})}{\partial y}\right)\right) - ghS_\mathrm{fy} \,, \end{aligned} \tag{3}$$

where (x, y) [m] are Cartesian coordinates and t [s] is the time coordinate. The variables $(q_\mathrm{x}, q_\mathrm{y}) = (uh, vh)$ [m^2/s] are the specific water discharges in the x and y direction, respectively, where h [m] is the flow depth and u [m/s] and v [m/s] are the depth-averaged flow velocities. The variable η [m] is the bed elevation and g [m/s^2] the acceleration due to gravity. The friction slopes are $(S_\mathrm{fx}, S_\mathrm{fy})$ [$-$] and the diffusion coefficient ν [m^2/s] is the horizontal eddy viscosity. The depth-averaging procedure of the equations of motion introduces terms that originate from the difference between the actual velocity at a certain elevation in the water column and the depth-averaged velocity. We separate the contributions due to turbulent motion and secondary flow caused by the flow curvature. The contribution due to turbulent motion is accounted for by the diffusion coefficient. *Elder* (1959) derived an expression for the diffusion coefficient that accounts for the effect of turbulent motion on the depth-averaged flow assuming a logarithmic profile for the primary flow and negligible effect of molecular viscosity:

$$\nu_\mathrm{E} = \frac{1}{6}\kappa h u^* \,, \tag{4}$$

where $\kappa = 0.41$ [−] is the Von Kármán constant and $u^* = \sqrt{C_f}Q/h$ [m/s] is the friction velocity. Parameter C_f [−] is a nondimensional friction coefficient, which we assume to be constant (*Ikeda et al.*, 1981; *Schielen et al.*, 1993) and $Q = \sqrt{q_x^2 + q_y^2}$ [m^2/s] is the module of the specific water discharge. In the numerical simulations we will assume the eddy viscosity to be a constant equal to the value given by ν_E in a reference state (e.g. *Falconer*, 1980; *Lien et al.*, 1999). Appendix A presents the limitations of the coefficient derived by *Elder* (1959).

The terms (F_{sx}, F_{sy}) [m^2/s^2] account for the effect of secondary flow. These terms are responsible for a transfer of momentum that shifts the maximum velocity to the outer bend (*Kalkwijk and De Vriend*, 1980), as well as for a sink of energy in the secondary circulation (*Flokstra*, 1977; *Begnudelli et al.*, 2010). We deal with these terms in Section 2.2.

We assume a Chézy-type friction:

$$S_{fx} = \frac{C_f q_x Q}{g h^3} , \quad S_{fy} = \frac{C_f q_y Q}{g h^3} . \tag{5}$$

One underlying assumption of the system of equations presented above is that the vertical length and velocity scales are negligible with respect to the horizontal ones. Another assumption is the fact that the concentration of sediment (the ratio between the solid and liquid discharge) is small (below 6×10^{-3} (*Garegnani et al.*, 2011, 2013)), such that we apply the clear water approximation.

2.2 Secondary Flow Equations

This section describes the equations that model secondary flow (i.e., formulations for F_{sx} and F_{sy} in equations (2) and (3)). The secondary flow velocity profile u^s [m/s] (i.e., the vertical profile of the velocity component perpendicular to the primary flow) is assumed to have a universal shape as a function of the relative elevation in the water column $\zeta = (z - \eta)/h$ [−], where z [m] is the vertical Cartesian coordinate perpendicular to x and y increasing in upward direction (*Rozovskii*, 1957; *Engelund*, 1974; *De Vriend*, 1977, 1981; *Booij and Pennekamp*, 1984). Worded differently, the vertical profile of the secondary flow is parametrised by a single value representing the intensity of the secondary flow I [m/s], such that $u^s = f(\zeta)I$. The secondary flow intensity I is the integral of the absolute value of the secondary flow velocity profile (*De Vriend*, 1981). Among others, *Rozovskii* (1957), *Engelund* (1974), and *De Vriend* (1977), derive equilibrium profiles of the secondary flow that differ in the description of the eddy viscosity, vertical profile of the primary flow, and the boundary condition of the flow at the bed. Following *De Vriend* (1977), we assume a logarithmic profile for the primary flow (i.e., a parabolic distribution of the eddy viscosity) and vanishing velocity close to the bed at $\zeta = \exp(-1 - 1/\alpha)$ where $\alpha = \frac{\sqrt{C_f}}{\kappa} < 0.5$.

The depth-averaging procedure yields the integral value (along z) of the force per unit mass that the secondary flow exerts on the primary flow (*De Vriend*, 1977; *Kalkwijk and De Vriend*,

1980):

$$F_{\mathrm{sx}} = \frac{\partial T_{\mathrm{xx}}}{\partial x} + \frac{\partial T_{xy}}{\partial y} \ , \tag{6}$$

$$F_{\mathrm{sy}} = \frac{\partial T_{\mathrm{yx}}}{\partial x} + \frac{\partial T_{\mathrm{yy}}}{\partial y} \ , \tag{7}$$

where T_{lm} [$\mathrm{m}^3/\mathrm{s}^2$] is the integral shear stress per unit mass in the direction l-m. Assuming a large width-to-depth ratio (i.e., $B/h \gg 1$, where B [m] is the characteristic channel width) and a mild curvature (i.e., $h/R_{\mathrm{s}} \ll 1$, where R_{s} [m] is the radius of curvature of the streamlines), the shear stress terms are:

$$T_{\mathrm{xx}} = -2\frac{\beta^* I}{Q} q_{\mathrm{x}} q_{\mathrm{y}} \ , \tag{8}$$

$$T_{\mathrm{xy}} = T_{\mathrm{yx}} = \frac{\beta^* I}{Q}\left(q_{\mathrm{x}}^2 - q_{\mathrm{y}}^2\right) \ , \tag{9}$$

$$T_{\mathrm{yy}} = T_{\mathrm{yy}} = 2\frac{\beta^* I}{Q} q_{\mathrm{x}} q_{\mathrm{y}} \ , \tag{10}$$

where $\beta^* = 5\alpha - 15.6\alpha^2 + 37.5\alpha^3$.

The simplest strategy to account for secondary flow assumes that the secondary flow is fully developed. This is equivalent to saying that the secondary flow intensity is equal to the equilibrium value $I_{\mathrm{e}} = Q/R_{\mathrm{s}}$ [m/s] found in an infinitely long bend (*Rozovskii*, 1957; *Engelund*, 1974; *De Vriend*, 1977, 1981; *Booij and Pennekamp*, 1983). A change in channel curvature leads to the streamwise adaptation of secondary flow to the equilibrium value (*De Vriend*, 1981; *Ikeda and Nishimura*, 1986; *Johannesson and Parker*, 1989; *Seminara and Tubino*, 1989). *Booij and Pennekamp* (1984) and *Kalkwijk and Booij* (1986) not only account for the spatial adaptation but also the temporal adaptation of the secondary flow associated with a variable discharge or tides. Here we adopt the latter strategy, which has been applied, for instance, in modelling the morphodynamics of braided rivers (*Javernick et al.*, 2016; *Williams et al.*, 2016; *Javernick et al.*, 2018). The spatial and temporal adaptation of secondary flow is expressed by (*Jagers*, 2003):

$$\frac{\partial I}{\partial t} + \frac{q_{\mathrm{x}}}{h}\frac{\partial I}{\partial x} + \frac{q_{\mathrm{y}}}{h}\frac{\partial I}{\partial y} - \frac{\partial}{\partial x}\left(\nu\frac{\partial I}{\partial x}\right) - \frac{\partial}{\partial y}\left(\nu\frac{\partial I}{\partial y}\right) = S_{\mathrm{s}} \ , \tag{11}$$

where S_{s} [m/s^2] is a source term which depends on the difference between the local secondary flow intensity and its equilibrium value:

$$S_{\mathrm{s}} = -\frac{I - I_{\mathrm{e}}}{T_{\mathrm{I}}} \ , \tag{12}$$

where T_{I} [s] is the adaptation time scale of the secondary flow:

$$T_{\mathrm{I}} = \frac{L_{\mathrm{I}} h}{Q} \ , \tag{13}$$

where $L_{\mathrm{I}} = L_{\mathrm{I}}^* h$ [m] is the adaptation length scale of the secondary flow, which depends on the nondimensional length scale $L_{\mathrm{I}}^* = \frac{1-2\alpha}{2\kappa^2\alpha}$ (*Kalkwijk and Booij*, 1986).

The radius of curvature of the streamlines is defined as (e.g. *Legleiter and Kyriakidis*, 2006):

$$\frac{1}{R_\mathrm{s}} = \frac{\frac{\mathrm{d}x}{\mathrm{d}t}\frac{\mathrm{d}^2y}{\mathrm{d}t^2} - \frac{\mathrm{d}y}{\mathrm{d}t}\frac{\mathrm{d}^2x}{\mathrm{d}t^2}}{\left(\left(\frac{\mathrm{d}x}{\mathrm{d}t}\right)^2 + \left(\frac{\mathrm{d}y}{\mathrm{d}t}\right)^2\right)^{3/2}} , \tag{14}$$

assuming steady flow and in terms of water discharge we obtain:

$$\frac{1}{R_\mathrm{s}} = \frac{-q_\mathrm{x}q_\mathrm{y}\frac{\partial q_\mathrm{x}}{\partial x} + q_\mathrm{x}^2\frac{\partial q_\mathrm{y}}{\partial x} - q_\mathrm{y}^2\frac{\partial q_\mathrm{x}}{\partial y} + q_\mathrm{x}q_\mathrm{y}\frac{\partial q_\mathrm{y}}{\partial y}}{\left(q_\mathrm{x}^2 + q_\mathrm{y}^2\right)^{3/2}} . \tag{15}$$

The secondary flow model described in this section closes the primary flow model described in Section 2.1 given a certain bed elevation. In the following section we describe the model equations that describe changes in bed elevation as a function of the primary and secondary flow.

2.3 Morphodynamic Equations

We consider an alluvial bed composed of an arbitrary number N of non-cohesive sediment fractions characterised by a grain size d_k [m], where the subscript k denotes the grain size fraction in increasing order (i.e., $d_1 < d_2 < ... < d_N$). Bed elevation change depends on the divergence of the sediment transport rate (*Exner*, 1920):

$$\frac{\partial \eta}{\partial t} + \frac{\partial q_\mathrm{bx}}{\partial x} + \frac{\partial q_\mathrm{by}}{\partial y} = 0 , \tag{16}$$

where $q_\mathrm{bx} = \sum_{k=1}^{N} q_{\mathrm{bx}k}$ [m^2/s] and $q_\mathrm{by} = \sum_{k=1}^{N} q_{\mathrm{by}k}$ [m^2/s] are the total specific (i.e., per unit of differential length) sediment transport rates including pores in the x and y direction, respectively. The variables $q_{\mathrm{bx}k}$ [m^2/s] and $q_{\mathrm{by}k}$ [m^2/s] are the specific sediment transport rates of size fraction k including pores. For simplicity we assume a constant porosity and density of the bed sediment. The sediment transport rate is assumed to be locally at capacity, which implies that we do not model the temporal and spatial adaptation of the sediment transport rate to capacity conditions (*Bell and Sutherland*, 1983; *Phillips and Sutherland*, 1989; *Jain*, 1992).

Changes in the bed surface grain size distribution are accounted for using the active layer model (*Hirano*, 1971). For simplicity, we assume a constant active layer thickness L_a [m]. Conservation of sediment mass of size fraction k in the active layer reads:

$$\frac{\partial M_{\mathrm{a}k}}{\partial t} + f_k^\mathrm{I}\frac{\partial \eta}{\partial t} + \frac{\partial q_{\mathrm{bx}k}}{\partial x} + \frac{\partial q_{\mathrm{by}k}}{\partial y} = 0 \quad k \in \{1, N-1\} , \tag{17}$$

and in the substrate (*Chavarrías et al.*, 2018):

$$\frac{\partial M_{sk}}{\partial t} - f_k^\mathrm{I}\frac{\partial \eta}{\partial t} = 0 \quad k \in \{1, N-1\} , \tag{18}$$

where $M_{ak} = F_{ak} L_a$ [m] and $M_{sk} = \int_{\eta_0}^{\eta_0+\eta-L_a} f_{sk}(z)\mathrm{d}z$ [m] are the volume of sediment of size fraction k per unit of bed area in the active layer and the substrate, respectively. Parameter η_0 [m] is a datum for bed elevation. Parameters $F_{ak} \in [0,1]$, $f_{sk} \in [0,1]$, and $f_k^I \in [0,1]$ are the volume fraction content of sediment of size fraction k in the active layer, substrate, and at the interface between the active layer and the substrate, respectively. By definition, the sum of the volume fraction content over all size fractions equals 1:

$$\sum_{k=1}^{N} F_{ak} = 1 \ , \quad \sum_{k=1}^{N} f_{sk}(z) = 1 \ , \quad \sum_{k=1}^{N} f_k^I = 1 \ . \tag{19}$$

Under degradational conditions, the volume fraction content of size fraction k at the interface between the active layer and the substrate is equal to that at the top part of the substrate ($f_k^I = f_{sk}(z = \eta - L_a)$ for $\partial\eta/\partial t < 0$). This allows for modelling of arbitrarily abrupt changes in grain size due to erosion of previous deposits. Under aggradational conditions the sediment transferred to the substrate is a weighted mixture of the sediment in the active layer and the bed load (*Parker*, 1991; *Hoey and Ferguson*, 1994; *Toro-Escobar et al.*, 1996). Here we simplify the analysis and we assume that the contribution of the bed load to the depositional flux is negligible (i.e., $f_k^I = F_{ak}$ for $\partial\eta/\partial t > 0$) (*Hirano*, 1971).

The magnitude of the sediment transport rate is assumed to be a function of the local bed shear stress. We apply the sediment transport relation by *Engelund and Hansen* (1967) in a fractional manner (*Blom et al.*, 2016, 2017) as well as the one by *Ashida and Michiue* (1971) (Appendix B).

The direction of the sediment transport (φ_{sk} [rad]) is affected by the secondary flow and the bed slope (*Van Bendegom*, 1947):

$$\tan\varphi_{sk} = \frac{\sin\varphi_\tau - \frac{1}{g_{sk}}\frac{\partial\eta}{\partial y}}{\cos\varphi_\tau - \frac{1}{g_{sk}}\frac{\partial\eta}{\partial x}} \quad k \in \{1, N\} \ , \tag{20}$$

where g_{sk} [$-$] is a function that accounts for the influence of the bed slope on the sediment transport direction and φ_τ [rad] is the direction of the sediment transport accounting for the secondary flow only:

$$\tan\varphi_\tau = \frac{q_y - h\alpha_I \frac{q_x}{Q} I}{q_x - h\alpha_I \frac{q_y}{Q} I} \ . \tag{21}$$

Assuming a mild curvature, uniform flow conditions, and a logarithmic profile of the primary flow, the constant α_I [$-$] is (*De Vriend*, 1977):

$$\alpha_I = \frac{2}{\kappa^2}(1-\alpha) \ . \tag{22}$$

The effect of the bed slope on the sediment transport direction depends on the grain size (*Parker*

and Andrews, 1985). We account for this effect setting:

$$g_{sk} = A_s \theta_k^{B_s} \quad k \in \{1, N\} \,, \tag{23}$$

where A_s [−] and B_s [−] are nondimensional parameters and θ_k [−] is the *Shields* (1936) stress (Appendix B). Different values of the coefficients A_s and B_s have been proposed (for a recent review, see *Baar et al.* (2018)). We consider two possibilities: (1) $A_s = 1$, $B_s = 0$ (*Schielen et al.*, 1993) and (2) $A_s = 1.70$ and $B_s = 0.5$ (*Talmon et al.*, 1995). In the first and simpler case, the bed slope effect is independent from the bed shear stress (*Engelund and Skovgaard*, 1973; *Engelund*, 1975). In the second, more complex, case, the bed slope effect is assumed to be dependent on the fluid drag force on the grains, which is assumed to depend on the Shields stress (*Koch and Flokstra*, 1981).

2.4 Linearised System of Equations

The system of equations describing the flow, change of bed level, and change of the bed surface texture is highly non-linear. Here we linearise the system of equations to provide insight on the fundamental properties of the model and to study the stability of perturbations. To this end we consider a reference state that is a solution to the system of equations. The reference state is a steady uniform straight flow in the x direction over an inclined plane bed composed of an arbitrary number of size fractions. Mathematically: $h_0 = \text{ct.}$, $q_{x0} = \text{ct.}$, $q_{y0} = 0$, $I_0 = 0$, $\frac{\partial \eta}{\partial x} = \text{ct.} = \frac{-C_f q_{x0}^2}{g h_0^3}$, $\frac{\partial \eta}{\partial y} = 0$, $M_{ak0} = \text{ct.}\ \forall k \in \{1, N-1\}$, where ct. denotes a constant different from 0 and subscript 0 indicates the reference solution.

We add a small perturbation to the reference solution denoted by $'$ and we linearise the resulting system of equations. After substituting the reference solution we obtain a system of equations of the perturbed variables:

$$\frac{\partial \mathbf{Q}'}{\partial t} + \mathbf{D_{x0}} \frac{\partial^2 \mathbf{Q}'}{\partial x^2} + \mathbf{D_{y0}} \frac{\partial^2 \mathbf{Q}'}{\partial y^2} + \mathbf{A_{x0}} \frac{\partial \mathbf{Q}'}{\partial x} + \mathbf{A_{y0}} \frac{\partial \mathbf{Q}'}{\partial y} + \mathbf{B_0} \mathbf{Q}' = 0 \,, \tag{24}$$

where the vector of dependent variables is:

$$\mathbf{Q}' = \left[h', q_x', q_y', I', \eta', [M_{ak}'] \right]^\intercal \,, \tag{25}$$

where the square bracket indicates the vector character.

The diffusive matrix in x direction is:

$$\mathbf{D_{x0}} = \left[\begin{array}{ccccc:c} 0 & 0 & 0 & 0 & 0 & \mathbb{0} \\ 2\nu\frac{q_{\mathrm{x}0}}{h_0} & -2\nu & -\nu & 0 & 0 & \mathbb{0} \\ 0 & 0 & -\nu & 0 & 0 & \mathbb{0} \\ 0 & 0 & 0 & -\nu & 0 & \mathbb{0} \\ 0 & 0 & 0 & 0 & 0 & \mathbb{0} \\ \hdashline \mathbb{0} & \mathbb{0} & \mathbb{0} & \mathbb{0} & \mathbb{0} & \mathbb{0} \end{array}\right], \tag{26}$$

where $\mathbb{0}$ denotes the zero matrix. The diffusive matrix in y direction is:

$$\mathbf{D_{y0}} = \left[\begin{array}{cccc:c:c} 0 & 0 & 0 & 0 & 0 & \mathbb{0} \\ \nu\frac{q_{\mathrm{x}0}}{h_0} & -\nu & 0 & 0 & 0 & \mathbb{0} \\ \nu\frac{q_{\mathrm{x}0}}{h_0} & -\nu & -2\nu & 0 & 0 & \mathbb{0} \\ 0 & 0 & 0 & -\nu & 0 & \mathbb{0} \\ 0 & 0 & 0 & 0 & \left.\frac{\partial q_{\mathrm{by}}}{\partial\frac{\partial\eta}{\partial y}}\right|_0 & \mathbb{0} \\ \hdashline \mathbb{0} & \mathbb{0} & \mathbb{0} & \mathbb{0} & \left[\left.\frac{\partial q_{\mathrm{by}k}}{\partial\frac{\partial\eta}{\partial y}}\right|_0 - f^{\mathrm{I}}_{k0}\left.\frac{\partial q_{\mathrm{by}}}{\partial\frac{\partial\eta}{\partial y}}\right|_0\right] & \mathbb{0} \end{array}\right]. \tag{27}$$

The advective matrix in x direction is:

$$\mathbf{A_{x0}} = \left[\begin{array}{ccccc:c} 0 & 1 & 0 & 0 & 0 & \mathbb{0} \\ gh_0 - \left(\frac{q_{\mathrm{x}0}}{h_0}\right)^2 & 2\frac{q_{\mathrm{x}0}}{h_0} & 0 & 0 & gh_0 & \mathbb{0} \\ 0 & 0 & \frac{q_{\mathrm{x}0}}{h_0} & -\beta^* q_{\mathrm{x}0} & 0 & \mathbb{0} \\ 0 & 0 & -\frac{q_{\mathrm{x}0}}{h_0^2 L^*_{\mathrm{I}}} & \frac{q_{\mathrm{x}0}}{h_0} & 0 & \mathbb{0} \\ \left.\frac{-q_{\mathrm{x}0}}{h_0}\frac{\partial q_{\mathrm{bx}}}{\partial q_{\mathrm{x}}}\right|_0 & \left.\frac{\partial q_{\mathrm{bx}}}{\partial q_{\mathrm{x}}}\right|_0 & 0 & 0 & 0 & \left[\left.\frac{\partial q_{\mathrm{bx}}}{\partial M_{\mathrm{al}}}\right|_0\right] \\ \hdashline \left[\left.\frac{-q_{\mathrm{x}0}}{h_0}\frac{\partial q_{\mathrm{b}k}}{\partial q_{\mathrm{x}}}\right|_0 + f^{\mathrm{I}}_{k0}\left.\frac{q_{\mathrm{x}0}}{h_0}\frac{\partial q_b}{\partial q_{\mathrm{x}}}\right|_0\right] & \left[\left.\frac{\partial q_{\mathrm{bx}k}}{\partial q_{\mathrm{x}}}\right|_0 - f^{\mathrm{I}}_{k0}\left.\frac{\partial q_{\mathrm{bx}}}{\partial q_{\mathrm{x}}}\right|_0\right] & \mathbb{0} & \mathbb{0} & \mathbb{0} & \left[\left.\frac{\partial q_{\mathrm{bx}k}}{\partial M_{\mathrm{al}}}\right|_0 - f^{\mathrm{I}}_{k0}\left.\frac{\partial q_{\mathrm{bx}}}{\partial M_{\mathrm{al}}}\right|_0\right] \end{array}\right]. \tag{28}$$

The advective matrix in y direction is:

$$\mathbf{A_{y0}} = \left[\begin{array}{ccccc:c} 0 & 0 & 1 & 0 & 0 & \mathbb{0} \\ 0 & 0 & \frac{q_{\mathrm{x}0}}{h_0} & -\beta^* q_{\mathrm{x}0} & 0 & \mathbb{0} \\ gh_0 & 0 & 0 & 0 & gh_0 & \mathbb{0} \\ 0 & 0 & 0 & 0 & 0 & \mathbb{0} \\ 0 & 0 & \left.\frac{\partial q_{\mathrm{by}}}{\partial q_{\mathrm{y}}}\right|_0 & \left.\frac{\partial q_{\mathrm{by}}}{\partial I}\right|_0 & 0 & \mathbb{0} \\ \hdashline \mathbb{0} & \mathbb{0} & \left[\left.\frac{\partial q_{\mathrm{by}k}}{\partial q_{\mathrm{y}}}\right|_0 - f^{\mathrm{I}}_{k0}\left.\frac{\partial q_{\mathrm{by}}}{\partial q_{\mathrm{y}}}\right|_0\right] & \left[\left.\frac{\partial q_{\mathrm{by}k}}{\partial I}\right|_0 - f^{\mathrm{I}}_{k0}\left.\frac{\partial q_{\mathrm{by}}}{\partial I}\right|_0\right] & \mathbb{0} & \mathbb{0} \end{array}\right]. \tag{29}$$

The matrix of linear terms is:

$$\mathbf{B_0} = \left[\begin{array}{ccccc:c} 0 & 0 & 0 & 0 & 0 & \mathbb{0} \\ \frac{-3C_{\mathrm{f}}q_{\mathrm{x}0}^2}{h_0^3} & \frac{2C_{\mathrm{f}}q_{\mathrm{x}0}}{h_0^2} & 0 & 0 & 0 & \mathbb{0} \\ 0 & 0 & \frac{C_{\mathrm{f}}q_{\mathrm{x}0}}{h_0^2} & 0 & 0 & \mathbb{0} \\ 0 & 0 & 0 & \frac{q_{\mathrm{x}0}}{h_0^2 L_{\mathrm{I}}^*} & 0 & \mathbb{0} \\ 0 & 0 & 0 & 0 & 0 & \mathbb{0} \\ \hdashline \mathbb{0} & \mathbb{0} & \mathbb{0} & \mathbb{0} & \mathbb{0} & \mathbb{0} \end{array}\right] . \tag{30}$$

We assume that the perturbations can be represented as a Fourier series, which implies that they are piecewise smooth and bounded for $x = \pm\infty$. Using this assumption the solution of the perturbed system is expressed in the form of normal modes:

$$\mathbf{Q'} = \mathrm{Re}\left(\mathbf{V}\mathrm{e}^{\mathrm{i}(k_{\mathrm{wx}}+k_{\mathrm{wy}}-\omega t)}\right) , \tag{31}$$

where i is the imaginary unit, k_{wx} [rad/m] and k_{wy} [rad/m] are the real wave numbers in x and y direction, respectively, $\omega = \omega_{\mathrm{r}} + \mathrm{i}\omega_{\mathrm{i}}$ [rad/s] is the complex angular frequency, $\mathbf{V}$ is the complex amplitude vector, and Re denotes the real part of the solution (which we will omit in the subsequent steps). The variable ω_{r} is the angular frequency and ω_{i} the attenuation coefficient. A value of $\omega_{\mathrm{i}} > 0$ implies growth of perturbations and $\omega_{\mathrm{i}} < 0$ decay. Substitution of equation (31) in equation (24) yields:

$$[\mathbf{M_0} - \omega\mathbb{1}]\,\mathbf{V} = 0 , \tag{32}$$

where:

$$\mathbf{M_0} = \mathbf{D_{x0}}k_{\mathrm{wx}}^2\mathrm{i} + \mathbf{D_{y0}}k_{\mathrm{wy}}^2\mathrm{i} + \mathbf{A_{x0}}k_{\mathrm{wx}} + \mathbf{A_{y0}}k_{\mathrm{wy}} - \mathbf{B_0}\mathrm{i} , \tag{33}$$

and $\mathbb{1}$ denotes the unit matrix. Equation (32) is an eigenvalue problem in which the eigenvalues of $\mathbf{M_0}$ (as a function of the wave number) are the values of ω satisfying equation (32).

The solution of the linear model provides information regarding the development of small amplitude oscillations only, but for an arbitrary wave number. For this reason the linear model is convenient for studying the well-posedness of the model, which we will assess in the following section.

3 Instability, Hyperbolicity, and Ill-Posedness

Ill-posedness has been related to the system of governing equations losing its hyperbolic character. Stability analysis investigates growth and decay of perturbations of a base state. The two mathematical problems may seem unrelated but in fact they are strongly linked. In this section we clarify the terms unstable, hyperbolic, and ill-posed, and present the mathematical framework that we use to study the well-posedness of the system of equations.

A system is stable if perturbations to an equilibrium state decay and the solution returns to its original state. This is equivalent to saying that all possible combinations of wave numbers in the x and y directions yield a negative growth rate (ω_i, equation (31)). An example of a stable system in hydrodynamics is the inviscid Shallow Water Equations (iSWE) for a Froude number smaller than 2 (*Jeffreys*, 1925; *Balmforth and Mandre*, 2004; *Colombini and Stocchino*, 2005). In figure 1a we show the maximum growth rate of perturbations to a reference solution (Case I1, tables 1 and 2) of the iSWE on an inclined plane (i.e., the first 3 equations of the complete system, equation (24), with neither secondary flow nor diffusion). The growth rate is obtained numerically by computing the eigenvalues of the reduced matrix $\mathbf{M_0}$ (the first 3 rows and columns in equation (33)) for wave numbers between 0 and 250 rad/m, which is equivalent to wavelengths ($l_\mathrm{wx} = 2\pi/k_\mathrm{wx}$ and equivalently for y) down to 1 cm. Figure 1b presents the same information as figure 1a in terms of wavelength rather than wave number to better illustrate the behaviour for large wavelengths. The growth rate is negative for all wave numbers, which confirms that the iSWE for Fr < 2 yield a stable solution.

u [m/s]	v [m/s]	h [m]	C_f [−]
1	0	1	0.007

Table 1: Reference state.

Case	model	Fr	stability	mathematical character
I1	iSWE	0.32	stable	well-posed
B1	iSWE+Exner	0.32	unstable	well-posed
I2	iSWE	2.01	unstable	ill-posed

Table 2: Cases of a stable well-posed model (I1), an unstable well-posed model (B1), and an ill-posed model (I2). Case I2 has the same parameter values as Case I1 but for the mean flow velocity which is equal to 6.30 m/s.

A system is unstable when perturbations to an equilibrium state grow and the solution diverges from the initial equilibrium state. The growth of river bars is an example of an unstable system in river morphodynamics. A straight alluvial channel is stable if the width-to-depth ratio is sufficiently small and, above a certain threshold value, the channel becomes unstable and free alternate bars grow (*Engelund and Skovgaard*, 1973; *Fredsøe*, 1978; *Colombini et al.*, 1987; *Schielen et al.*, 1993).

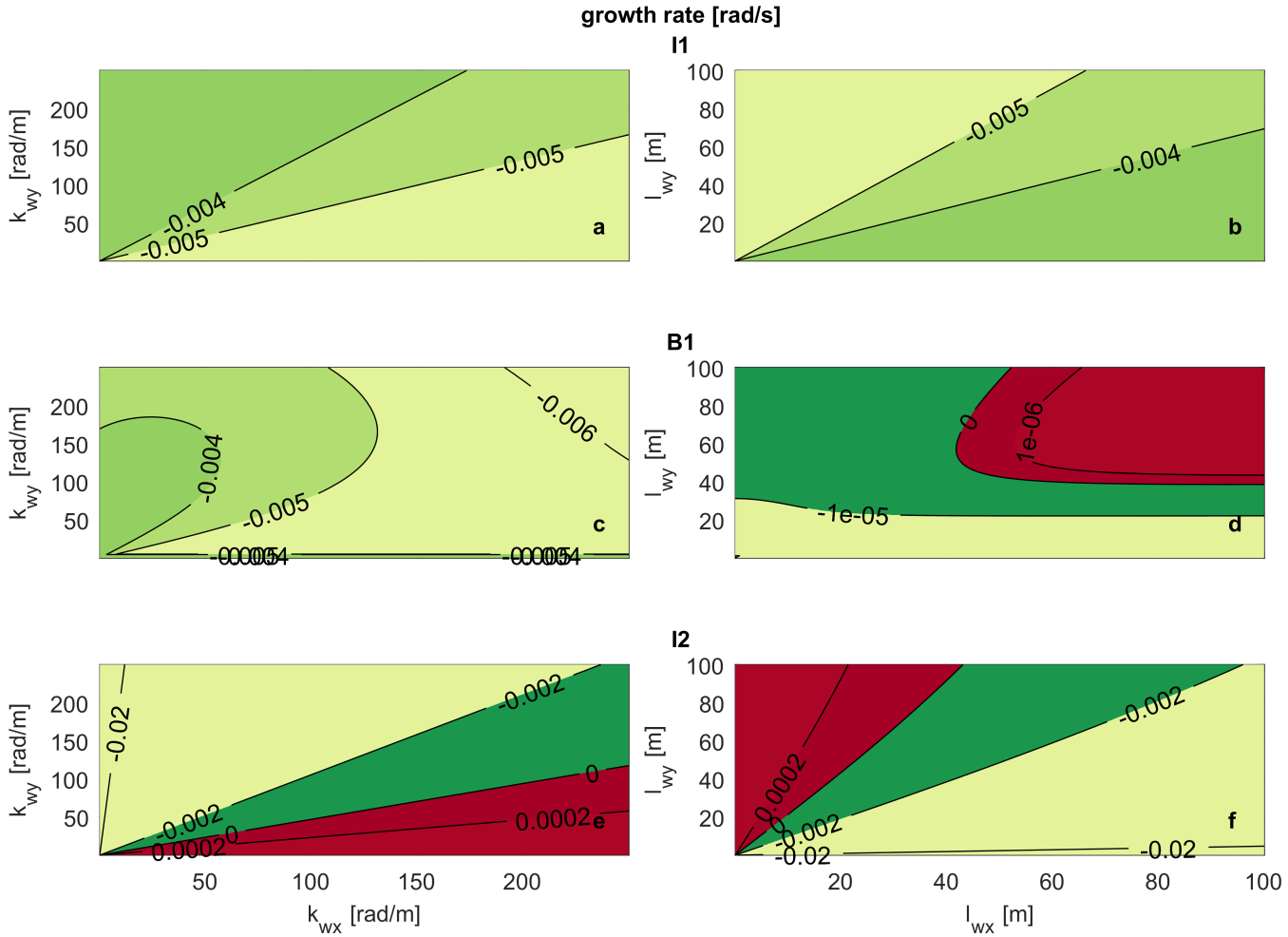

Figure 1: Growth rate of perturbations added to the reference case (tables 1 and 2) as a function of the wave number and the wavelength: (**a**)-(**b**) iSWE, Fr < 2 (Case I1, well-posed), (**c**)-(**d**) iSHE+Exner (Case B1, well-posed), and (**e**)-(**f**) iSWE, Fr > 2 (Case I2, ill-posed). The subplots in the two columns show the same information but highlight the behaviour for large wave numbers (left column) and for large wavelengths (right column). Red and green indicates growth and decay of perturbations, respectively.

Mathematically, an unstable system has a region, a domain in the wave number space, in which the growth rate of perturbations is positive. In figure 1c-d we present the growth rate of perturbations to a reference solution consisting of uniform flow (table 1) on an alluvial bed composed of unisize sediment with a characteristic grain size equal to 0.001 m (Case B1, table 2). The sediment transport rate is computed using the relation by *Engelund and Hansen* (1967) (equation (42)) and the effect of the bed slope on the sediment transport direction is accounted for using the simplest formulation, $g_s = 1$. Figure 1d confirms the classical result of linear bar theory: there exists a critical transverse wavelength (l_{wyc}) below which all perturbations decay. In our particular case $l_{wyc} = 40.2$ m. Impermeable boundary conditions at the river banks limit the possible wavelengths to fractions of the channel width B [m] such that $l_{wy} = 2B/m$ for $m = 1, 2, ...$ (*Callander*, 1969). As the most unstable mode is the first one (i.e., $m = 1$, alternate bars) (*Colombini et al.*, 1987; *Schielen et al.*, 1993), the minimum channel width above which perturbations grow is $B_c = l_{wyc}/2 = 20.1$ m,

which confirms the results of *Schielen et al.* (1993). Figure 1c highlights, as for case I1, the decay of short waves.

A particular case of instability is that in which the domain of positive growth rate extends to infinitely large wave numbers (i.e., short waves). Under this condition there is no cutoff wave number above which we can neglect the contribution of ever shorter waves with non-zero growth rates. For any unstable perturbation a shorter one can be found which is even more unstable. This implies that the growth rate of an infinitesimal perturbation (i.e., noise) tends to infinity. Such a system cannot represent a physical phenomenon, as the growth rate of any physical process in nature is bounded. A system in which the growth rate of infinitesimal perturbations tends to infinity does not have a unique solution depending continuously on the initial and boundary conditions, which implies that the system is ill-posed (*Hadamard*, 1923; *Joseph and Saut*, 1990). An example of an ill-posed hydrodynamic model is the iSWE for flow with a Froude number larger than 2. In figure 1e-f we show the growth rate of perturbations to the reference solution of a case in which the Froude number is slightly larger than 2 (Case I2, table 2). The growth rate extends to infinitely large wave numbers, which confirms that this case is ill-posed. A model being ill-posed is an indication that there is a relevant physical mechanism that has been neglected in the model derivation (*Fowler*, 1997). Viscous forces regularise the iSWE (i.e., make the model well-posed) and rather than ill-posed, the viscous Shallow Water Equations become simply unstable for a Froude number larger than 2, predicting the formation of roll-waves (*Balmforth and Mandre*, 2004; *Balmforth and Vakil*, 2012; *Rodrigues and Zumbrun*, 2016; *Barker et al.*, 2017a,b).

Chaotic models, just as ill-posed models, are sensitive to the initial and boundary conditions and lose their predictive capabilities in a deterministic sense (*Lorenz*, 1963). Yet, there are two essential differences. First, chaotic systems lose their predictive capabilities after a certain time (*Devaney*, 1989; *Banks et al.*, 1992), yet there exists a finite time in which the dynamics are predictable. In ill-posed models infinitesimal perturbations to the initial condition cause a finite divergence in the solution in an arbitrarily (but fixed) short time. Second, while the dynamics of a chaotic model are not predictable in deterministic terms after a certain time, these continue to be predictable in statistical terms. For this reason, although being sensitive to the initial and boundary conditions, a model presenting chaotic properties can be used, for instance, to capture the essential dynamics and spatio-temporal features of river braiding (*Murray and Paola*, 1994, 1997). On the contrary, the dynamics of an ill-posed model cannot be analysed in statistical terms.

The numerical solution of an ill-posed problem continues to change as the grid is refined because a smaller grid size resolves larger wave numbers with faster growth rates (*Joseph and Saut*, 1990; *Kabanikhin*, 2008; *Barker et al.*, 2015; *Woodhouse et al.*, 2012). In other words, the numerical solution of an ill-posed problem does not converge when the grid cell size is reduced. This property emphasizes the unrealistic nature of ill-posed problems and shows that ill-posed models cannot be applied in practice.

We present an example of grid dependence specifically related to river morphodynamics under conditions with mixed-size sediment. We consider a case of degradation into a substrate finer than the active layer, as this is a situation in which the active layer model is prone to be ill-posed (Section 1). The reference state is the same as in Case B1, yet the sediment is a mixture of two sizes equal to 0.001 m and 0.010 m. The bed surface is composed of 10 % of fine sediment. The active layer thickness is equal to 0.05 m, which in this case is representative of small dunes covering the bed (e.g. *Deigaard and Fredsøe*, 1978; *Armanini and Di Silvio*, 1988; *Blom*, 2008). Depending on the substrate composition, this situation yields an ill-posed model (*Chavarrías et al.*, 2018). When the substrate is composed of 50 % of fine sediment (Case H1, table 3), the problem is well-posed and it is ill-posed when the substrate is composed of 90 % of fine sediment (Case H2, table 3).

We use the software package Delft3D (*Lesser et al.*, 2004) to solve the system of equations. We stress that the problem of ill-posedness is inherent to the system of equations and independent from the numerical solver. We have implemented a subroutine that assesses the well-posedness of the system of equations at each node and time step. The domain is 100 m long and 10 m wide. The downstream water level is lowered at a rate of 0.01 m/h to induce degradational conditions. The upstream sediment load is constant and equal to the equilibrium value of the reference state (*Blom et al.*, 2017). The cells are square and we consider three different sizes (table 3). The time step varies between simulations to maintain a constant value of the CFL number.

Case	f_1^{I} [−]	Δx [m]	mathematical character
H1a	0.5	0.50	well-posed
H1b	0.5	0.25	well-posed
H1c	0.5	0.10	well-posed
H2a	0.9	0.50	ill-posed
H2b	0.9	0.25	ill-posed
H2c	0.9	0.10	ill-posed

Table 3: Cases showing the effect of grid cell size on the numerical solution of well-posed and ill-posed models.

Figure 2 presents the bed elevation after 10 h. The result of the well-posed case (H1, left column) is grid independent. The result of the ill-posed case (H2, right column) changes as the grid is refined and presents an oscillatory pattern characteristic of ill-posed simulations (*Joseph and Saut*, 1990; *Woodhouse et al.*, 2012; *Barker et al.*, 2015; *Chavarrías et al.*, 2018). The bed seems to be flat in the ill-posed simulation with a coarser grid (figure 2b). This is because oscillations grow slowly on a coarse grid and require more time to be perceptible. The waviness of the bed is seen in the result of the check routine, as it predicts ill-posedness only at those locations where the bed degrades (the stoss face of the oscillations). The fact that the model is well-posed in almost the entire domain in the ill-posed case solved using a cell sizes equal to 0.25 m (H2b, figure 2d) and 0.10 m (H2c, figure 2f) does not mean that the results are realistic. Non-physical oscillations have grown and vertically mixed the sediment such that the situation is well-posed after 10 h (*Chavarrías*

et al., 2018). We provide a movie of figure 2 in the online supplementary material.

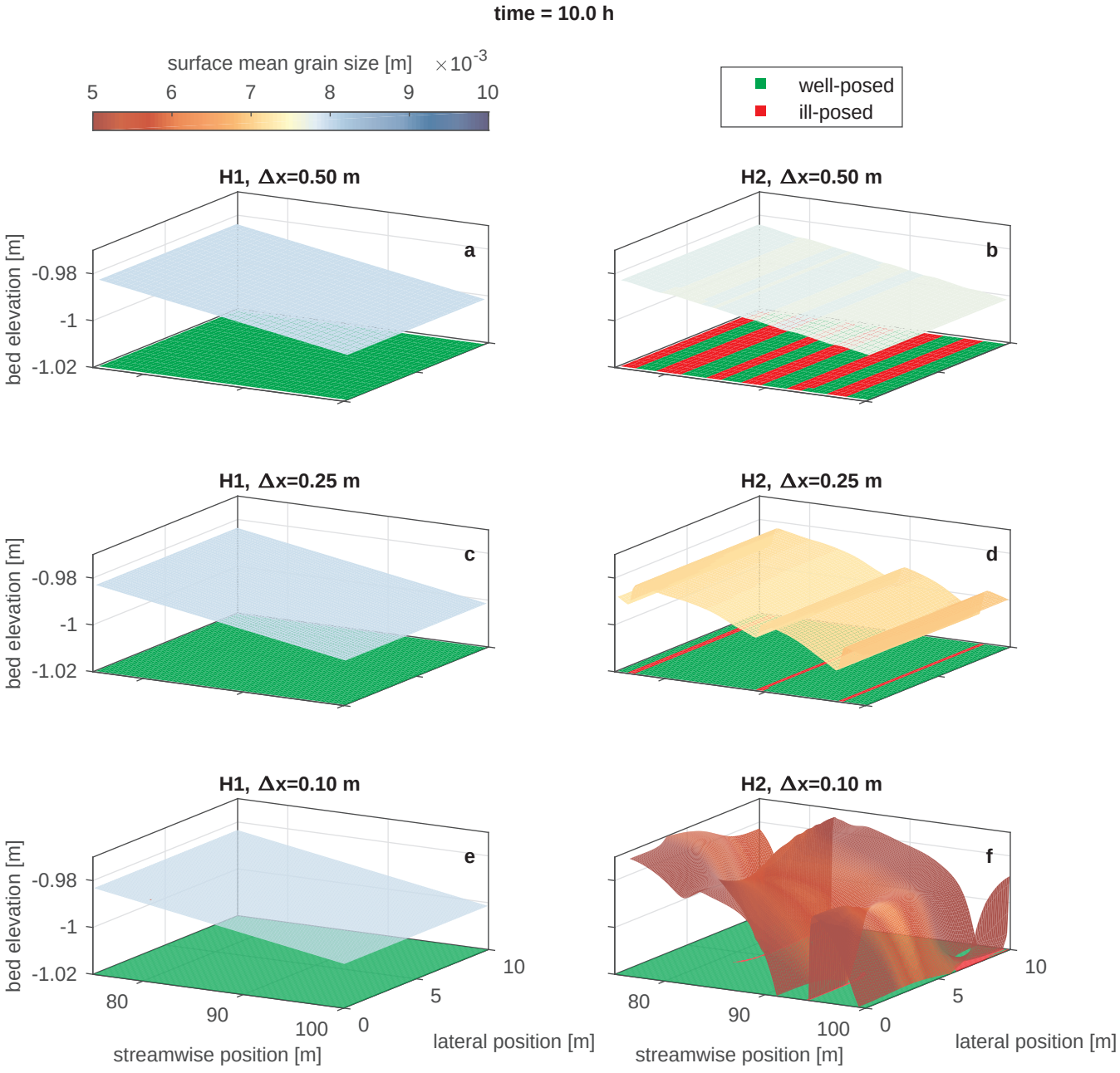

Figure 2: Simulated bed elevation (surface) and mean grain size at the bed surface (colour) of a well-posed case (left column, H1, table 3) and an ill-posed case (right column, H2, table 3). In each row we present the results for varying cell size. The colour of the $x-y$ plane shows the result of the routine that checks whether the conditions at each node yield a well-posed (green) or an ill-posed (red) model.

In the above idealised situations it is evident that the oscillations are non-physical and it is straightforward to do a converge test to clarify that the solution is grid dependent. In complex domains in which several processes play a role, it is more difficult to associate oscillations to ill-posedness. Moreover, in long term applications the growth rate of perturbations may be fast compared to the frequency at which model results are assessed, which may hide the consequences

of ill-posedness. If one studies a process that covers months or years (and consequently analyses the results on a monthly basis) but perturbations due to ill-posedness grow on an hourly scale, it may be difficult to identify that the problem is ill-posed. Using poor numerical techniques to solve the system of equations also contributes to hiding the consequences of ill-posedness as numerical diffusion dampens perturbations. These factors may explain why the problem of ill-posedness in mixed-sediment river morphodynamics is not widely acknowledged.

In the river morphodynamics community, the term ellipticity has been used to refer to ill-posedness of the system of equations in contrast to hyperbolicity, which is associated to well-posedness (*Ribberink*, 1987; *Mosselman*, 2005; *Stecca et al.*, 2014; *Siviglia et al.*, 2017; *Chavarrías et al.*, 2018). In general the terms are equivalent, but not always. We consider a unit vector $\hat{n}$ in the direction (x, y), $\hat{n} = (\hat{n_{\mathrm{x}}}, \hat{n_{\mathrm{y}}})$. The system of equations (24) is hyperbolic if matrix $\mathbf{A} = \mathbf{A_{x0}}\hat{n_{\mathrm{x}}} + \mathbf{A_{y0}}\hat{n_{\mathrm{y}}}$ diagonalises with real eigenvalues $\forall \hat{n}$ (e.g. *LeVeque*, 2004; *Castro et al.*, 2009). Neglecting friction and diffusive processes (i.e., $\mathbf{B_0} = \mathbf{D_{x0}} = \mathbf{D_{y0}} = \mathbb{0}$), hyperbolicity implies that the eigenvalues of $\mathbf{M_0}$ (equation (33)) are real. In this case, as the growth rate of perturbations (i.e., the imaginary part of the eigenvalues of $\mathbf{M_0}$) is equal to 0 regardless of the wave number, the system of equations is well-posed. As the coefficients of $\mathbf{A}$ are real, complex eigenvalues appear in conjugate pairs. This means that if $\mathbf{A}$ has a complex eigenvalue (i.e., the problem is not hyperbolic), at least one wave will have a positive growth rate. Neglecting friction and diffusive processes, non-hyperbolicity implies that infinitely large wave numbers have a positive growth rate. We conclude that, in the absence of diffusion and friction, lack of hyperbolicity implies ill-posedness. Note that ellipticity (i.e., the eigenvalues of $\mathbf{A}$ are all complex) is not required for the problem to be ill-posed, as it suffices that the problem is not hyperbolic. When considering diffusion and friction even when $\mathbf{A}$ has complex eigenvalues, the imaginary part of the eigenvalues of $\mathbf{M_0}$ may all be negative and the problem well-posed.

Finally, well-posedness and hyperbolicity are similar terms when dealing with problems arising from conservation laws and changes with time, as hyperbolicity guarantees the existence of wave solutions (*Lax*, 1980; *Courant and Hilbert*, 1989; *Strikwerda*, 2004; *Toro*, 2009; *Dafermos*, 2010; *Bressan*, 2011; *Dafermos*, 2016). In communities such as materials science, it is the term hyperbolicity that is associated to ill-posedness, as a smooth solution of, for instance the stress, requires that the system is elliptic (*Knowles and Sternberg*, 1975, 1976; *Veprek et al.*, 2007).

4 Stability Analysis

In this section we study the applicability of the system of equations to model two-dimensional river morphodynamics by means of a stability analysis of perturbations. We study the effects of the secondary flow model (Sections 4.1) and the bed slope (Section 4.2) on model ill-posedness.

4.1 Ill-Posedness Due to Secondary Flow

In this section we study how the stability of the system of equations is affected by the secondary flow model. To gain insight we compare three cases. In the first case we omit secondary flow. In the second and third cases we include the secondary flow model with and without considering diffusion (table 4).

Case	secondary flow	ν	stability	mathematical character
S1	no	ν_E	stable	well-posed
S2	yes	ν_E	unstable	well-posed
S3	yes	0	unstable	ill-posed

Table 4: Variations to the reference state (table 1) and results of the linear analysis with respect to secondary flow.

The first case is equivalent to I1 (table 2), yet the eddy viscosity is equal to the value derived by *Elder* (equation (4), $\nu = \nu_E = 0.0057\,\mathrm{m}^2/\mathrm{s}$). In figure 3a-b we plot the maximum growth rate of perturbations as a function of the wave number and the wavelength, respectively. Diffusion appears to significantly dampen perturbations (compare figure 1a in which diffusion is neglected to figure 3a).

In the second case we repeat the analysis including the equation for advection and diffusion of the secondary flow intensity (i.e., the first 4 rows and columns of matrix $\mathbf{M_0}$ in equation (33), Case S2, table 4). We observe that accounting for secondary flow introduces an instability mechanism (figure 3d). For the specific conditions of the case, a growth domain appears for wavelengths between 0.7 m and 39 m long and between 0.4 m and 19 m wide. The maximum growth corresponds to a wavelength in the x and y direction equal to 1.29 m and 0.74 m, respectively. This situation is well-posed, as for large wave numbers perturbations decay (figure 3c). Yet, the model is unsuitable for reproducing such instability, as it predicts growth of perturbations with a length scale of the order of the flow depth and shorter, for which the SWE model is not suited. Given the fact that we consider a depth-averaged formulation of the primary flow, processes that scale with the flow depth are not resolved by the model and consequently perturbations at that scale must decay to yield physically realistic results. Otherwise, scales of the order of the flow depth become relevant, which contradicts the assumptions of the depth-averaged formulation. To model processes that scale with the flow depth such as dune growth, it is necessary to account for non-depth-averaged flow formulations that consider, for instance, rotational flow (*Colombini and Stocchino*, 2011, 2012), or non-hydrostatic pressure (*Giri and Shimizu*, 2006; *Shimizu et al.*, 2009).

In the third case we test the secondary flow model without accounting for diffusion in the system of equations ($\nu = 0$, Case S3, table 4). We observe that the instability domain extends to infinitely large wave numbers (figure 3e), which implies that this model is ill-posed (Section 3). We now aim to prove that the Shallow Water Equations in combination with the secondary flow model without

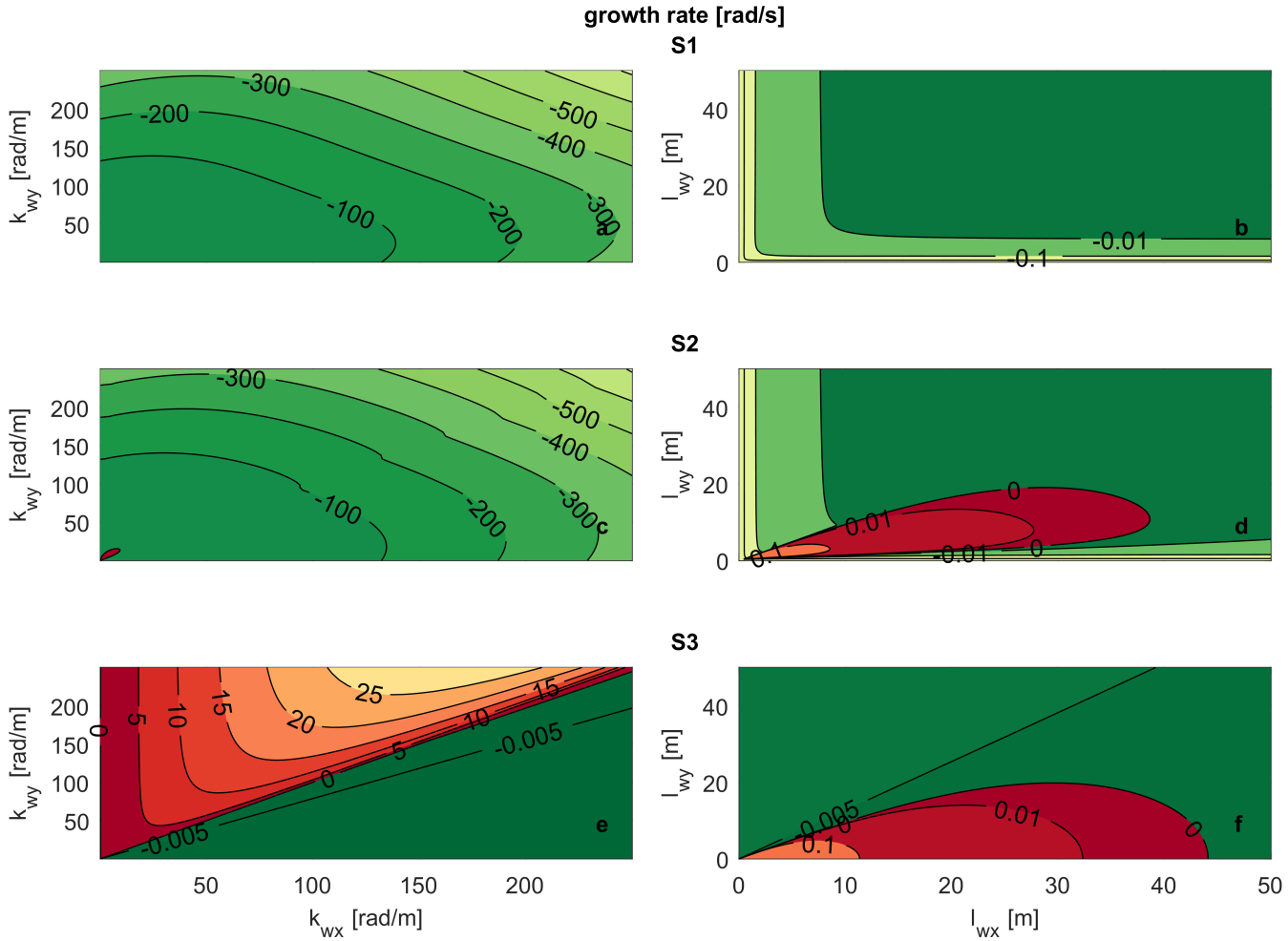

Figure 3: Growth rate of perturbations added to the reference case (tables 1 and 4) as a function of the wave number and the wavelength: (**a**)-(**b**) without secondary flow (Case S1, well-posed), (**c**)-(**d**) accounting for secondary flow with diffusion (Case S2, well-posed), and (**e**)-(**f**) accounting for secondary flow without diffusion (Case S3, ill-posed). The subplots in the two columns show the same information but highlight the behaviour for large wave numbers (left column) and for large wavelengths (right column). Red and green indicates growth and decay of perturbations, respectively.

diffusion always yields an ill-posed model. To this end we obtain the characteristic polynomial of matrix $\mathbf{M_0}$ (equation (33)). We compute the discriminant of the fourth order characteristic polynomial and we find that for $k_{\mathrm{wx}} < k_{\mathrm{wy}}$ the growth rate of perturbations is positive (Appendix C). The model is ill-posed, as there always exists a domain of growth extending to infinitely large wave numbers in the transverse direction.

We assess how the length scale of the instability related to the secondary flow model depends on the flow parameters. For this purpose we compute the shortest wave with positive growth for a varying diffusion coefficient and flow conditions (figure 4). We observe that, independently from the flow conditions, the theoretical value of the diffusion coefficient derived by *Elder* (1959) (equation (4)) is insufficient for dampening oscillations scaling with the flow depth. We conclude that if the diffusion coefficient is realistic, the treatment of the secondary flow yields an unrealistic model. It is necessary to use an unrealistically large value of the diffusion coefficient to obtain a

realistic depth-averaged model in which perturbations scaling with the flow depth decay.

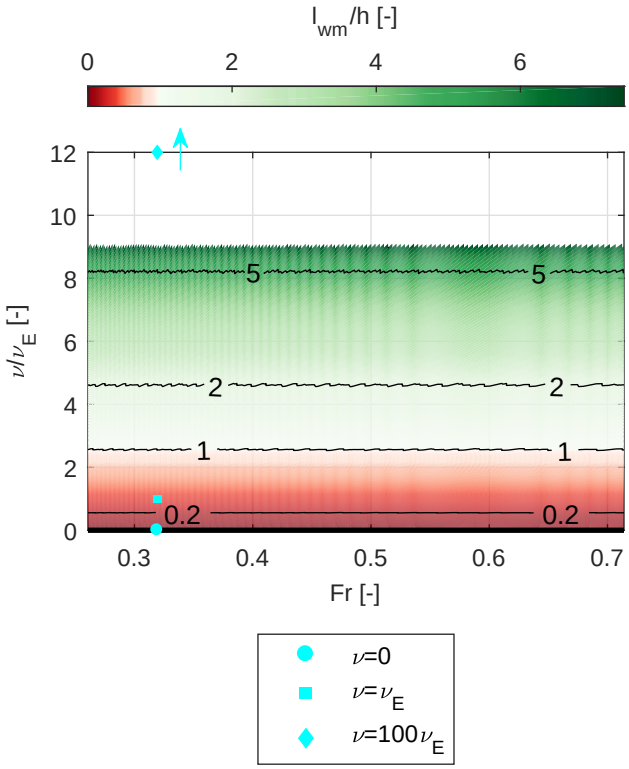

Figure 4: Wavelength of the shortest perturbation with positive growth rate (l_{wm}) relative to the flow depth (h) as a function of the Froude number (Fr) and the diffusion coefficient (ν) relative to the diffusion coefficient according to *Elder* (1959) (ν_{E}). Different flow conditions are studied varying the flow depth between 0.2 m and 1.5 m from the reference case (table 1). The cyan markers indicate the conditions of three numerical simulations with different values of the diffusion coefficient (Section 5.1). The arrow next to the diamond marker indicates that the value lies outside the figure. Red (green) colours indicate that the shortest wave length with positive growth rate are smaller (larger) than the flow depth.

4.2 Ill-Posedness Due to Bed Slope Effect

In this section we study the influence of considering the effect of the bed slope on model well-posedness. To gain insight we compare 5 cases in which we consider unisize and mixed-size sediment, various sediment transport relations, and various bed slope functions (table 5). We neglect secondary flow and diffusion to reduce the complexity of the problem (*Parker*, 1976; *Fredsøe*, 1978; *Colombini et al.*, 1987; *Schielen et al.*, 1993).

Our reference case is B1 (Section 3) which considers unisize sediment conditions, and the effect of the bed slope on the sediment transport direction is accounted for using the simplest formulation, $g_{\mathrm{s}} = 1$. We have shown that this case is well-posed. Neglecting the effect of the bed slope on the sediment transport direction (Case B2, table 5) makes the problem ill-posed (figure 5a). This illustrates that accounting for the effect of the bed slope is required for obtaining not only physically realistic but also mathematically well-posed results. We prove that the Shallow

Water Equations in combination with the *Exner* (1920) equation without considering the effect of the bed slope always yields an ill-posed model by studying the growth rate of perturbations in the limit for the wave number k_{wy} tending to infinity (Appendix D).

Case	sediment	d_2 [m]	sed. trans.	bed slope	mathematical character
B1	unisize	-	EH	$g_{\mathrm{s}} = 1$	well-posed
B2	unisize	-	EH	No	ill-posed
B3	mixed-size	0.004	AM	$g_{sk} = 1$	well-posed
B4	mixed-size	0.004	AM	$g_{sk} = 1.7\theta_k^{0.5}$	ill-posed
B5	mixed-size	0.012	AM	$g_{sk} = 1$	ill-posed

Table 5: Variations to the reference state (table 1) and results of the linear analysis with respect to the effect of the bed slope on the sediment transport direction. EH and AM refer to the sediment transport relations by *Engelund and Hansen* (1967) and *Ashida and Michiue* (1971), respectively.

The fact that the bed slope effect dampens perturbations under unisize conditions is expected from the fact that the only diffusive term in the system of equations is $\partial q_{\mathrm{by}}/\partial s_{\mathrm{y}}$ (equation (27)), where $s_{\mathrm{y}} = \partial\eta/\partial y$. This term is negative and approximately equal to $-q_{\mathrm{b}}/g_{\mathrm{s}}$ for a small streamwise slope. When we consider more than one grain size, diffusive terms appear in each active layer equation. We find that these diffusive terms may be positive, which hints at the possibility of an antidiffusive behaviour, which may lead to ill-posedness. To study this possibility we compute the growth rate of perturbations of a simplified case consisting of two sediment size fractions. In the limit for the wave numbers tending to infinity, the maximum growth rate is:

$$\omega_{\mathrm{i}}^{\mathrm{lim}} = \alpha_1 \left(r_{\mathrm{y1}} - d_{\mathrm{x1,1}}\right)^2 + \alpha_2 \left(r_{\mathrm{y1}} - d_{\mathrm{x1,1}}\right) + \alpha_3 \ , \tag{34}$$

where α_i for $i = 1, 2, 3$ are parameters relating the flow and the sediment transport rate (Appendix E). The parameter r_{y1} explains how the sediment transport rate of the fine fraction is affected by changes in the transverse bed slope:

$$r_{\mathrm{y1}} = \frac{\partial q_{\mathrm{by1}}/\partial s_{\mathrm{y}}}{\partial q_{\mathrm{by}}/\partial s_{\mathrm{y}}} \ , \tag{35}$$

and the parameter $d_{\mathrm{x1,1}}$ relates changes in the sediment transport rate to changes in the volume of sediment in the active layer:

$$d_{\mathrm{x1,1}} = \frac{\partial q_{\mathrm{bx1}}/\partial M_{\mathrm{a1}}}{\partial q_{\mathrm{bx}}/\partial M_{\mathrm{a1}}} \ . \tag{36}$$

As $\alpha_1 > 0$ (Appendix E), there exist an interval $\left(r_{\mathrm{y1}} - d_{\mathrm{x1,1}}\right)^- < \left(r_{\mathrm{y1}} - d_{\mathrm{x1,1}}\right) < \left(r_{\mathrm{y1}} - d_{\mathrm{x1,1}}\right)^+$ in which $\omega_{\mathrm{i}}^{\mathrm{lim}} < 0$ and the model is well-posed. Outside the interval, $\omega_{\mathrm{i}}^{\mathrm{lim}} > 0$ and the problem is ill-posed.

The physical interpretation of the limit values for obtaining a well-posed model is as follows. The effect of the transverse bed slope (r_{y1}) needs to be balanced with respect to the effect of changes in surface texture ($d_{\mathrm{x1,1}}$) to obtain a well-posed model. For a given $d_{\mathrm{x1,1}}$, if parameter

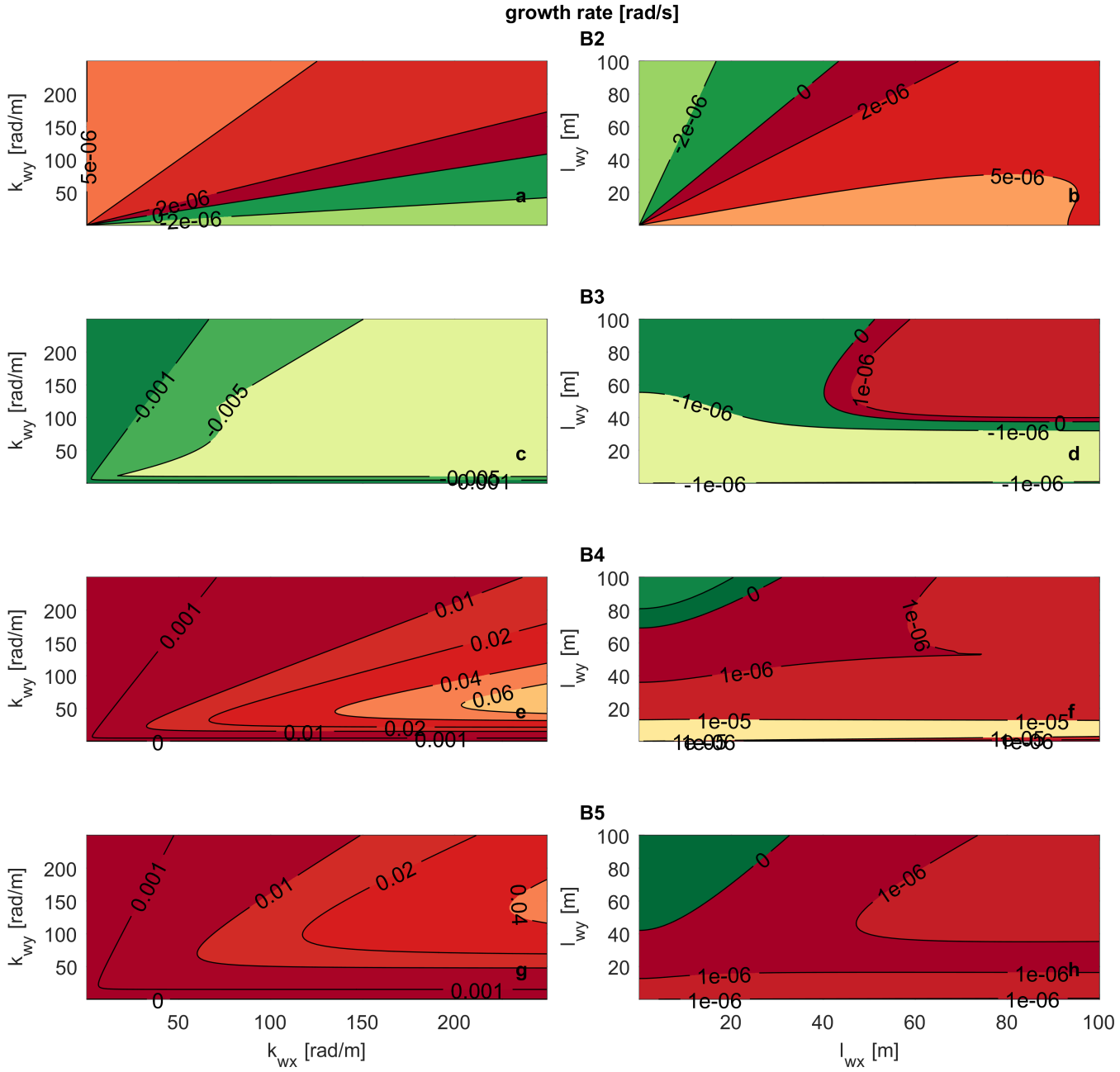

Figure 5: Growth rate of perturbations added to the reference case (tables 1 and 5) as a function of the wave number and the wavelength: (**a**)-(**b**) Case B2 (ill-posed), (**c**)-(**d**) Case B3 (well-posed), (**e**)-(**f**) Case B4 (ill-posed), and (**g**)-(**h**) Case B5 (ill-posed). The subplots in the two columns show the same information but highlight the behaviour for large wave numbers (left column) and for large wavelengths (right column). Red and green indicates growth and decay of perturbations, respectively.

r_{y1} is too small (i.e., the bed slope effect is not sufficiently strong) perturbations in the transverse direction are not dampened and the model is ill-posed. On the other hand, for a given r_{y1}, if parameter $d_{x1,1}$ is too small (e.g. due to relatively strong hiding or in conditions close to incipient motion) perturbations in the streamwise direction do not decay and the model is also ill-posed. The critical values $r_{y1}^{\pm}$ that allow for a well-posed model are shown in Appendix E.

In Cases B3-B5 we illustrate the possibility of ill-posedness due to the bed slope closure relation

(table 5). In Case B3 the sediment mixture consists of two grain size fractions with characteristic grain sizes equal to 0.001 m and 0.004 m. The volume fraction content of the fine sediment in the active layer and at the interface between the active layer and the substrate is equal to 0.5. The sediment transport rate is computed using the relation developed by *Ashida and Michiue* (1971). The other parameters are equal to the reference case (table 1). The system is well-posed when the effect of the bed slope does not depend on the bed shear stress (figure 5c). The situation is ill-posed if the effect of the bed slope depends on the bed shear stress (Case B4, table 5, figure 5e). The cause of ill-posedness is not found in the closure relation for the bed slope effect only but in the combination of the closure relation with the flow and bed surface conditions. A case equal to B3 except for the fact that the coarse grain size is equal to 0.012 m is ill-posed (Case B5, table 5, figure 5g).

We assess how the domain of ill-posedness due to the bed slope effect depends on the model parameters. For given sediment sizes, flow, and bed surface texture, parameter B_s (equation (23)) controls the effect of the bed slope by modifying $r_{\mathrm{y}1}$ only. The parameter A_s (equation (23)) cancels in $r_{\mathrm{y}1}$ and does not play a role. For this reason we study how g_{s1}/A_s $[-]$ affects the domain of ill-posedness for varying sediment properties, flow, and bed surface grain size distribution (figure 6). We consider Case B3 and we vary B_s between 0 and 0.5 to vary the bed slope effect. The sediment size of the coarse fraction varies between d_1 and 0.020 m. The mean flow velocity varies between 1 m/s and 2.8 m/s. The volume fraction content of fine sediment at the bed surface varies between 0 and 1. We aim to isolate the problem of ill-posendess due to bed slope effect from the problem of ill-posedness due to a different grain size distribution at the bed surface and at the interface between the bed surface and the substrate (*Chavarrías et al.*, 2018). For this reason, in this analysis the volume fraction content of fine sediment at the interface is equal to the one at the bed surface. Under this condition the problem can be ill-posed due to the effect of the bed slope only.

As we have shown analytically, under unisize conditions (i.e., $d_1/d_2 = 1$ or $F_{\mathrm{a}1} = 1$ or $F_{\mathrm{a}1} = 0$) the model is well-posed (figure 6a and 6c). For sufficiently different grain sizes ($d_1/d_2 \lessapprox 0.15$) the model is well-posed regardless of the bed slope effect but for a small range of values ($0.08 \lessapprox d_1/d_2 \lessapprox 0.1$). This small range of ill-posed values is associated with $r_{\mathrm{y}1}$ increasing for decreasing values of d_1/d_2 and acquiring a value larger than $r_{\mathrm{y}1}^+$ such that the model becomes ill-posed for all values of the bed slope effect. A further decrease in d_1/d_2 increases the limit value $r_{\mathrm{y}1}^+$ faster than $r_{\mathrm{y}1}$ such that the model becomes well-posed for all values of the bed slope effect.

An increase in the Froude number decreases the domain of well-posedness, which is explained from the fact that an increase in Froude number decreases $r_{\mathrm{y}1}$ while it does not modify $r_{\mathrm{y}1}^-$. We have assumed steady flow in deriving $\omega_\mathrm{i}^\mathrm{lim}$ to reduce the complexity of the model such that we can find an analytical solution (Appendix E). This causes a physically unrealistic resonance phenomenon for $\mathrm{Fr} \to 1$ (*Colombini and Stocchino*, 2005). In reality we do not expect that for Fr=1 the model is

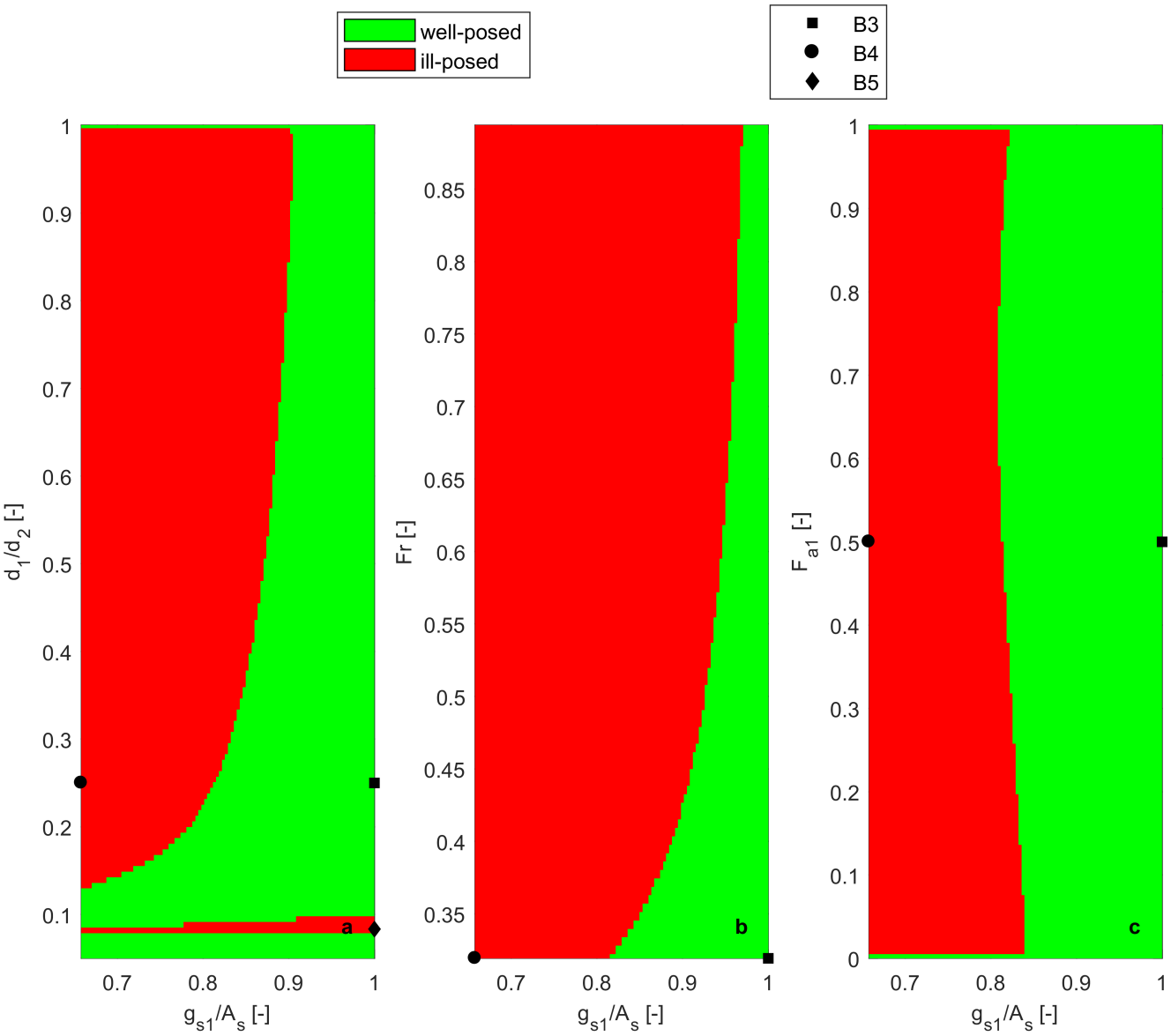

Figure 6: Domain of ill-posedness due to the bed slope effect under mixed-size sediment conditions: as a function of the ratio between fine and coarse sediment (**a**), the Froude number (**b**), and the volume fraction content of fine sediment in the active layer (**c**). The bed slope effect is measured by g_{s1}/A_s and the range of parameters is obtained by varying B_s (equation (23)). The range of values of d_1/d_2 is obtained by varying d_2. The range of values of the Froude number is obtained by varying u. The volume fraction content of fine sediment at the interface between the active layer and the substrate is kept equal to the volume fraction content of fine sediment in the active layer. The conditions represent unisize sediment when $d_1/d_2 = 1$, $F_{a1} = 0$, or $F_{a1} = 1$.

always ill-posed regardless of the bed slope effect. Apart from the limit values in which the problem becomes unisize, the surface volume fraction content does not significantly affect the domain of ill-posedness (figure 6c) as it rescales in more or less a similar way $r_{y1}^{\pm}$ and r_{y1}.

While Case B4 is ill-posed because the effect of the bed slope (r_{y1}) is small, Case B5 is ill-posed because parameter $d_{x1,1}$ is small. The different origin of ill-posedness does not cause a significant difference in the growth rate of perturbations as a function of the wave number (figure 5e-g). However, we will find out that the pattern resulting from the perturbations depends on the origin

of ill-posedness.

5 Application

The results of the linear stability analysis (Section 4) neglect second order terms and non-linear interactions. In this section we study the effects of the terms neglected in the linear analysis and the development of perturbations by means of numerical simulations. We use the software package Delft3D (*Lesser et al.*, 2004). This exercise provides information on the consequences of ill-posedness in numerical simulations and clarifies the limitations of the current modelling approach. We study the effect of secondary flow (Section 5.1) and the bed slope effect (Section 5.2).

5.1 Secondary Flow

We run 5 numerical simulations with a fixed bed (i.e., only the flow is computed) to study the role of the secondary flow model and the diffusion coefficient on the ill-posedness of the system of equations. The first 3 simulations reproduce the conditions of Cases S1, S2, and S3 (table 4). The domain is rectangular, 100 m long and 10 m wide. We use square cells with size equal to 0.1 m. The time step is equal to 0.01 s and we simulate 10 minutes of flow. We set a constant water discharge and the downstream water level remains constant with time. The initial condition represents normal flow for the values in table 1 (i.e., equilibrium conditions).

The simulation not accounting for secondary flow does not present growth of perturbations as predicted by the linear analysis and remains stable with time (figure 7a). We observe growth of perturbations when we account for secondary flow with the diffusion coefficient derived by *Elder* (1959) (figure 7b). The results are physically unrealistic as the flow depth presents variations of up to 7 % of the normal flow depth and the length scale of perturbations is smaller than the flow depth. We have not introduced any perturbation in the initial or boundary conditions which implies that perturbations grow from numerical truncation errors. This supports the fact that the simulation is physically unrealistic. The case with a diffusion coefficient equal to 0 is ill-posed and the solution presents unreasonably large oscillations (figure 7c). These numerical results confirm the results of the linear stability analysis.

In the fourth simulation we set a diffusion coefficient 100 times larger than the one derived by *Elder* (1959) (figure 7d). Under this condition the linear analysis predicts all short waves to decay (diamond in figure 4). These numerical results confirm the linear theory. The last simulation is equal to Case S2 except for the fact that we use a coarser grid ($\Delta x = \Delta y = 1\,\mathrm{m}$). In this case the numerical grid is not sufficiently detailed for resolving the perturbations due to secondary flow and the simulation is stable (figure 7e). This last case highlights an important limitation of a physically unrealistic model. Although Case S2 is mathematically well-posed, the solution presents similarities with ill-posed cases in the sense that a refinement of the grid causes non-physical oscillations to

appear.

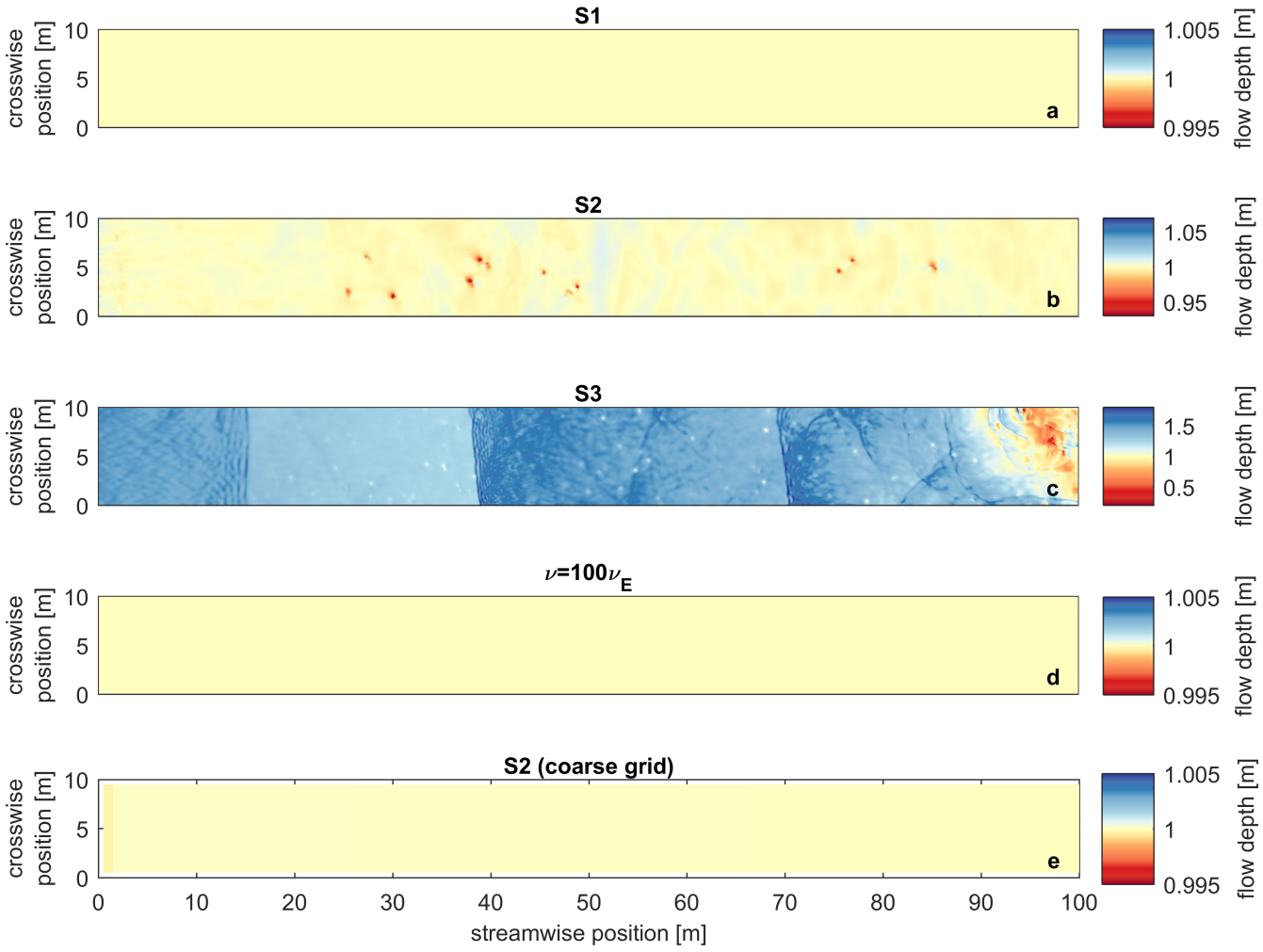

Figure 7: Flow depth at the end of the simulations: (**a**) without accounting for secondary flow (Case S1), (**b**) setting $\nu = \nu_{\mathrm{E}}$ (Case S2), (**c**) setting $\nu = 0$ (Case S3), (**d**) setting $\nu = 100\nu_{\mathrm{E}}$, and (**e**) setting $\nu = \nu_{\mathrm{E}}$ using a coarser numerical grid (Case S2). The colour map is adjusted for each case and centred around the initial and equilibrium value ($h = 1\,\mathrm{m}$).

5.2 Bed Slope Effect

In this section we focus on the consequences of accounting for the bed slope effect on the mathematical character of the model. To this end we run 5 more numerical simulations without accounting for secondary flow and updating the bed (i.e., accounting for morphodynamic change). The simulations reproduce Cases B1-B5 (table 5). We simulate 8 h using a time step $\Delta t = 0.1\,\mathrm{s}$.

We have proved that accounting for the effect of the bed slope makes a unisize simulation well-posed (Section 4.2 and figure 1c). The numerical solution of this case (B1, table 2) is stable and perturbations do not grow (figure 8a). Moreover, no alternate bars appear as the channel width is below the critical value (Section 3). Perturbations grow when the effect of the bed slope is not taken into account (Case B2, figure 8b), which confirms that this case is ill-posed.

The mixed-size sediment conditions of Case B3 yield a well-posed model (figure 5e) and the

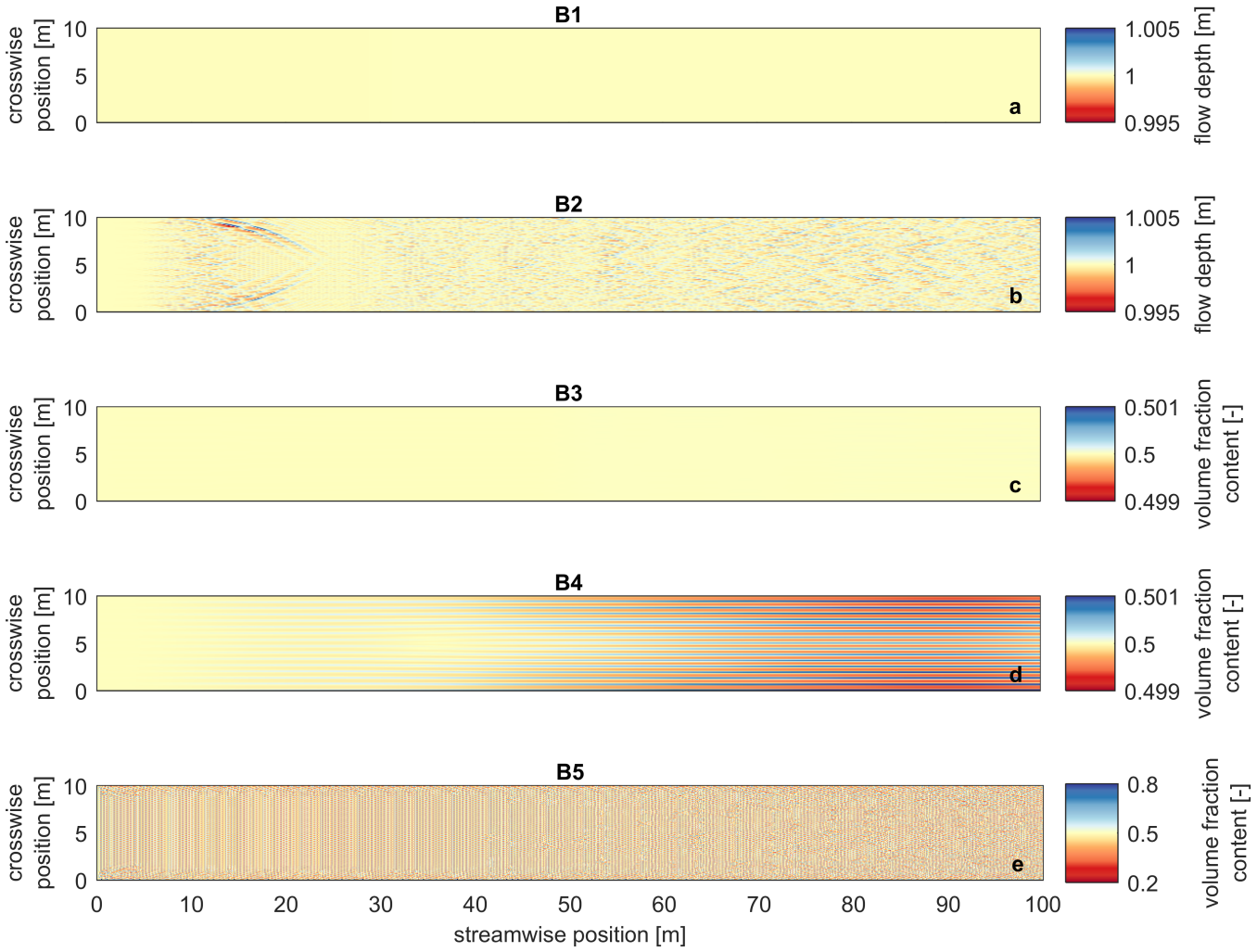

Figure 8: Flow depth at the end of the simulations of: (**a**) Case B1, (**b**) Case B2; and volume fraction content of fine sediment in the active layer: (**c**) Case B3, (**d**) Case B4, (**e**) Case B5. The colour map is adjusted for each case and centred around the initial and equilibrium value.

simulation is stable (figure 8c). On the other hand, the ill-posed cases B4 and B5 present growth of unrealistic and non-physical perturbations (figure 8d-e). While the growth of perturbations in Case B5 seems random, in Case B4 we observe a clear pattern. Moreover, oscillations have grown significantly faster in Case B5 than in Case B4. While after 8 h the changes in volume fraction content at the bed surface are of the order of 10^{-3} in Case B4, these are of order 1 in Case B5.

The fact that oscillations grow faster in Case B5 than in Case B4 is related to the different origin of ill-posedness. While Case B4 is ill-posed because the effect of the bed slope is not sufficiently strong (i.e., $r_{y1} < r_{y1}^{-}$), Case B5 is ill-posed because changes in the sediment transport rate due to changes in the volume of fine sediment in the active layer are too small (i.e., $r_{y1} > r_{y1}^{+}$). The first case is closely linked to the lateral direction, in which sediment transport is initially zero. The fact that initially the lateral sediment transport rate is zero limits the rate at which lateral changes occur. In the second case perturbations are linked to the streamwise direction, in which the sediment transport rate initially is non-zero, which enhances the rate at which changes develop.

6 Discussion

The origin of the instability due to secondary flow is found in the source term (S_s in equation (11)). As the source term depends on the flow curvature, the source term is 0 in a straight flow. A small perturbation in the flow causes the flow to curve. The flow curvature causes a source of secondary flow intensity, which further increases the flow curvature, causing a positive feedback. The flow curvature is largest for the smallest perturbations, which explains why the model is ill-posed if a dampening mechanism (i.e., diffusion) is not taken into account. This destabilizing mechanism may seem plausible to explain secondary flow circulation observed in straight channels (*Nikuradse*, 1930; *Brundrett and Baines*, 1964; *Nezu and Nakagawa*, 1984; *Gavrilakis*, 1992). However, secondary flow in a straight channel can only be caused by anisotropy of turbulence (*Einstein and Li*, 1958; *Gessner and Jones*, 1965; *Bradshaw*, 1987; *Colombini*, 1993), which is not included in the model for secondary flow. For this reason, the secondary flow model must predict decay of secondary flow intensity in case of straight flow. Diffusion of secondary flow intensity causes decay of perturbations, but the theoretical diffusion coefficient derived by *Elder* (1959) appears to be insufficient to dampen perturbations.

The advection equation of the secondary flow intensity was initially derived for steady decaying secondary flow on a straight reach after a bend neglecting the effect of diffusion (*De Vriend*, 1981). It is assumed that the same advective behaviour is valid for a varying curvature (*De Vriend*, 1981; *Olesen*, 1982) and in an unsteady situation (*Booij and Pennekamp*, 1984). These assumptions have, to our knowledge, not been tested. Moreover, secondary flow affects the vertical profile of the primary flow. This feedback mechanism, which limits the development of secondary flow (*Blanckaert and De Vriend*, 2004; *Blanckaert*, 2009), is not included in the model. *Blanckaert and de Vriend* (2003), *Blanckaert and Graf* (2004) and *Ottevanger et al.* (2013) propose non-linear models that take into consideration this mechanism. We expect that accounting for the feedback mechanism yields a well-posed model.

The feedback mechanism between the secondary and the primary flow may be seen as an increase of diffusivity, as it causes an enhanced momentum redistribution. For a situation in which the non-linear model for the secondary flow appears to be excessively expensive in computational terms, a diffusion coefficient depending on the secondary flow intensity would (partially) account for the enhanced momentum redistribution and provide a well-posed and realistic model.

We have assumed that the diffusion coefficient is constant and equal in all directions, which is a crude approximation, as in the streamwise direction diffusion is larger than in the transverse direction (Appendix A). It would be interesting to study the effect of anisotropic diffusion, however, we do not expect that this will significantly alter our results. This is because a larger diffusion coefficient in the streamwise direction will not alter the most unstable wavelength in the lateral direction. For this reason the shortest unstable waves remain to be of the order of the flow depth.

The non-linear relation between the flow and the sediment transport rate causes the growth of perturbations in bed elevation. Worded differently, a deep flow attracts the flow and vice versa, which enhances the growth of perturbations. This mechanism is counteracted by the bed slope effect, which causes deep parts to fill in. In this sense, it seems logical that it is necessary to account for bed slope effects to obtain a well-posed model. This may be confirmed by the facts that *Parker* (1976), by not considering the bed slope effect, found that all streams tend to form bars and, similarly, *Olesen* (1982) concluded that "the stream will develop an infinite number of submerged bars". From our point of view the fact that all streams seem to be unstable and develop an infinite number of submerged bars is a consequence of the model being ill-posed. Our analysis shows that the bed slope effect is a crucial physical process in analysing two-dimensional morphodynamic processes.

Nevertheless, the numerical simulations by *Qian et al.* (2016) of bar development without accounting for the bed slope effect do not show unrealistic oscillatory behaviour as is characteristic of ill-posedness. Yet, there is an essential difference between their model and the one we analyse here. We do not model the interaction between the sediment in the bed and the sediment in transport as we assume that the sediment transport rate adapts instantaneously to changes in the flow (i.e., the sediment transport rate depends on the flow variables only). Essentially, sediment in transport is not conserved and bed elevation and surface texture changes depend on the divergence of the sediment transport rate at capacity conditions. *Qian et al.* (2016) account for the conservation of mass of the sediment in transport and use an entrainment-deposition formulation for modelling bed elevation and surface texture changes (*Parker et al.*, 2000). In this formulation changes depend on the difference between the rate at which sediment is entrained from the bed and at which it is deposited on the bed. The fact that their model does not show symptoms of ill-posedness, while the effect of the bed slope is not taken into consideration, raises the question whether the entrainment-deposition formulation in combination with mass conservation of the sediment in transport is responsible, like the bed slope effect, for a mechanism that counteracts growth of perturbations in bed elevation. If the model used by *Qian et al.* (2016) is indeed well-posed, the effect of the bed slope may be a crucial process only when mass conservation of the sediment in transport is not considered.

Lanzoni and Tubino (1999) investigated the development of alternate bars under mixed-size sediment conditions using a model similar to the one we apply here. They assumed secondary flow to be negligible and considered a different set of closure relations for friction, the sediment transport rate, and the effect of the bed slope. Under the conditions they studied, they found that, similarly to the unisize case, growth of perturbations occurs if the width-to-depth ratio is above a critical value. This implies that they found that their model is well-posed, as short wave length perturbations decay. Given that the essence of the closure relations they considered is the same as the ones considered here and there is no fundamental difference, we suppose that their

model may become ill-posed if different conditions are studied (i.e., different flow or sediment parameters). This is because well-posedness is not related to the model equations only, but also to the conditions in which the model is applied.

The bed slope effect (represented by the parameter r_{y1}) needs to be balanced with respect to the effect of changes in the bed surface grain size distribution (represented by $d_{x1,1}$) to yield a well-posed model. The balance depends on the flow and bed conditions. For this reason, a particular closure relation may yield an ill-posed model in some subdomain of a simulation and a well-posed model in some other subdomain. It is necessary to further study the development of the transverse bed slope under mixed-size sediment conditions (e.g. *Baar et al.*, 2018) to obtain a universally applicable closure relation.

Overall, there are three causes of ill-posedness of the model: (1) the secondary flow parametrisation, (2) the closure relation for the bed slope effect, and (3) the representation of the vertical mixing processes when using the active layer model (*Ribberink*, 1987; *Chavarrías et al.*, 2018). We summarise all the conditions in which the model may become ill-posed in figure 9.

Only in idealised simulations it is straightforward to relate instability of the system of equations to ill-posedness. We advocate for an *a priori* test of whether the system of equations is well-posed or ill-posed, especially when dealing with mixed-size sediment cases. If at some time a location in the model becomes ill-posed, the model results should be carefully evaluated. The fact that some domain area has always been well-posed does not guarantee a unique solution, as oscillations caused by upstream or downstream ill-posed areas propagate through the domain. Similarly, the fact that the entire domain is well-posed at some time is no guarantee of a unique solution, as past oscillations due to ill-posedness affect the present solution.

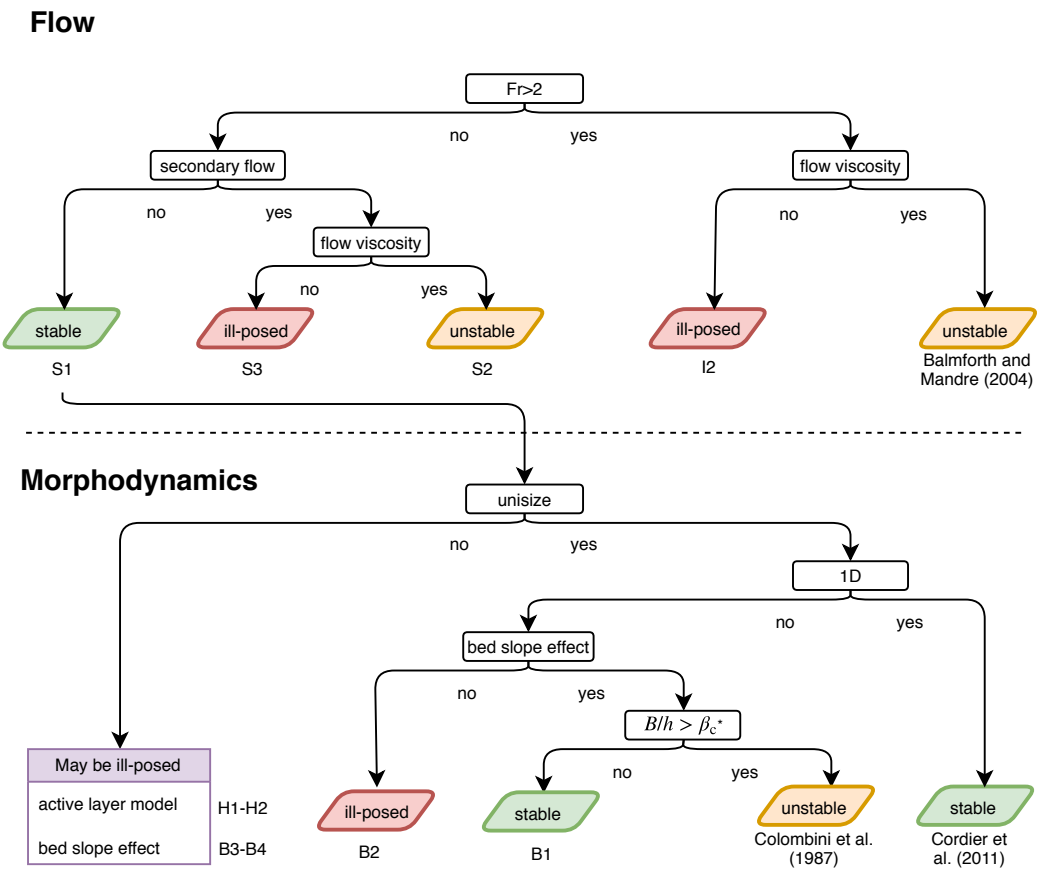

Figure 9: Conditions in which the flow model (top) and the morphodynamic model (bottom) is stable, unstable, or ill-posed. The code below the model type (e.g., S1) indicates an example case of such a situation. See tables 2, 3, 4, and 5 for an explanation of the cases S1-3, B1-4, H1-2, and I2. * Parameter β_c denotes the critical width-to-depth ratio (*Engelund and Skovgaard*, 1973; *Colombini et al.*, 1987; *Schielen et al.*, 1993).

7 Conclusions

We have studied a two-dimensional system of equations used to model mixed-size river morphodynamics as regards to its well-posedness. The model is based on the depth-averaged Shallow Water Equations in combination with the *Exner* (1920) and active layer (*Hirano*, 1971) equations to model bed elevation and surface texture changes, respectively. In particular we have focused on modelling of the secondary flow induced by flow curvature and the effect of the bed slope on the sediment transport direction, which causes particles to deviate from the direction of the bed shear stress.

By means of a linear stability analysis of the system of equations we find that:

- The parametrisation accounting for secondary flow yields an ill-posed model if diffusion is not accounted for.
- The theoretical amount of diffusion due to depth-averaging the vertical profile of the primary flow (*Elder*, 1959) yields a well-posed model but it predicts growth of perturbations that are incompatible with the shallow water assumption.

- The effect of the bed slope on the direction of the sediment transport is a necessary mechanism for the model being well-posed. Yet, a different modelling strategy accounting for conservation of the sediment in transport and an entrainment-deposition formulation may yield a well-posed model without accounting for the effect of the bed slope.

- Not all closure relations accounting for the bed slope effect are valid under mixed-size sediment conditions. There needs to be a balance between the effect of the bed slope and the effect of the streamwise variation of grain size distribution on the sediment transport rate.

Numerical simulations of idealised cases confirm the above results of the linear stability analysis.

Acknowledgements

The fruitful discussions and comments on the manuscript of Liselot Arkesteijn and insights from Mart Borsboom are gratefully acknowledged. We thank the editor Neil J. Balmforth, Marco Colombini, and two anonymous reviewers for their suggestions, which have significantly improved the manuscript.

A Eddy Viscosity

In general terms, given the anisotropy of the flow field, the diffusion tensor has non-diagonal terms and the diagonal terms are not equal (i.e., the diffusion coefficient in the streamwise direction ν_s is different than in the transverse direction ν_n). The non-diagonal terms become significant close to corners (*Fischer*, 1973) but far from corners the diagonal terms dominate. *Elder* (1959) derived an eddy viscosity coefficient in the streamwise and lateral direction assuming a logarithmic profile for the primary flow:

$$\nu_\mathrm{s} = \left(\frac{0.4041}{\kappa^3} + \frac{1}{6}\kappa\right) hu^* \,, \tag{37}$$

$$\nu_\mathrm{n} = \frac{1}{6}\kappa h u^* \,. \tag{38}$$

Elder neglected the effect of the viscous sublayer, which causes his analytical expression to be a lower limit of the diffusion coefficient (*Fischer*, 1967).

Several researchers (e.g. *Erdogan and Chatwin*, 1967; *Simons and Albertson*, 1963; *Fischer*, 1969; *Holley*, 1971; *Fischer*, 1973; *Kyong and Il*, 2016) propose values for the diffusion coefficient that are significantly larger than the one derived by *Elder* (1959). These values are used, for instance, by *Parker* (1978); *Ikeda and Nishimura* (1985) and *Van Prooijen and Uijttewaal* (2002). These values of the diffusion coefficient are derived from experimental measurements and implicitly account for the enhanced momentum redistribution due to secondary flow that we account for by means of the dispersive stresses.

In numerical simulations resolving the secondary flow, the diffusion coefficients derived by *Elder* (1959) are valid if the grid is of the order of magnitude of the flow depth (assuming that the relevant turbulent processes scale with the flow depth). Otherwise the numerical grid filters out significant two-dimensional turbulent motions that need to be accounted for in the closure model (*Talstra*, 2011). In our numerical runs the grid cell size is always smaller than the flow depth.

B Magnitude of the Sediment Transport Rate

The module of the specific sediment transport rate of size fraction k, $q_{\mathrm{b}k}$ [m^2/s], has a direction given by the angle $\varphi_{\mathrm{s}k}$ [rad]:

$$(q_{\mathrm{bx}k}, q_{\mathrm{by}k}) = q_{\mathrm{b}k}(\cos\varphi_{\mathrm{s}k}, \sin\varphi_{\mathrm{s}k}) \ . \tag{39}$$

The magnitude of the sediment transport rate is equal to:

$$q_{\mathrm{b}k} = F_{\mathrm{a}k}\sqrt{gRd_k^3}\,(1-p)\,q^*_{\mathrm{b}k} \ , \tag{40}$$

where p is the porosity and $q^*_{\mathrm{b}k}$ [$-$] is a nondimensional sediment transport rate (*Einstein*, 1950) dependent on the *Shields* (1936) stress:

$$\theta_k = \frac{C_{\mathrm{f}}\left(\frac{Q}{h}\right)^2}{gRd_k} \ . \tag{41}$$

The parameter $R = \rho_{\mathrm{s}}/\rho_{\mathrm{w}} - 1$ [$-$] is the submerged sediment density, $\rho_{\mathrm{s}} = 2650\,\mathrm{kg/m^3}$ is the sediment density and $\rho_{\mathrm{w}} = 1000\,\mathrm{kg/m^3}$ is the water density. To compute the nondimensional sediment transport rate we use a fractional form (*Blom et al.*, 2016, 2017) of the relation proposed by *Engelund and Hansen* (1967) neglecting form drag:

$$q^*_{\mathrm{b}k} = \frac{0.05}{C_{\mathrm{f}}}\theta_k^{5/2} \ , \tag{42}$$

and the relation including a nondimensional critical shear stress θ_{c} [$-$] proposed by *Ashida and Michiue* (1971):

$$q^*_{\mathrm{b}k} = 17\,(\theta_k - \xi_k\theta_{\mathrm{c}})\left(\sqrt{\theta_k} - \sqrt{\xi_k\theta_{\mathrm{c}}}\right) \ . \tag{43}$$

The parameter ξ_k [$-$] is the hiding factor that accounts for the fact that fine sediment in a mixture hides behind larger grains and a coarse sediment in a mixture is more exposed than in unisize

coarse sediment (*Einstein*, 1950). *Ashida and Michiue* (1971) proposes $\theta_c = 0.05$ and the relation:

$$\xi_k = \begin{cases} 0.843 \left(\frac{d_k}{D_m}\right)^{-1} & \text{for } \frac{d_k}{D_m} \leq 0.4 \\ \left(\frac{\log_{10}(19)}{\log_{10}(19\frac{d_k}{D_m})}\right)^2 & \text{for } \frac{d_k}{D_m} > 0.4 \end{cases} , \tag{44}$$

where D_m is a characteristic mean grain size of the sediment mixture.

C Proof of Ill-posedness Due to Secondary Flow without Diffusion

In this section we prove that the model based on the Shallow Water Equations accounting for secondary flow without diffusion is ill-posed.

The system of equations is composed of the first four rows and columns of the full system of equations in equation (24). Neglecting diffusive processes matrices $\mathbf{D_{x0}}$ and $\mathbf{D_{y0}}$ are equal to $\mathbb{0}$. As we are interested in the short-wave domain, friction can be neglected. The resulting matrix $\mathbf{M_0}$ of the linearised eigenvalue problem (equation (33)) is:

$$\mathbf{M_0} = \mathbf{A_{x0}} k_{wx} + \mathbf{A_{y0}} k_{wy} . \tag{45}$$

We compute the fourth order characteristic polynomial of matrix $\mathbf{M_0}$. The roots of the characteristic polynomial are the eigenvalues (i.e., the angular frequencies ω in equation (31)). The discriminant of a fourth order polynomial $p(\omega) = p_4\omega^4 + p_3\omega^3 + p_2\omega^2 + p_1\omega + p_0 = 0$ is equal to (*Beeler et al.*, 1972):

$$\begin{aligned} \Delta_4 = &(p_1^2p_2^2p_3^2 - 4p_1^3p_3^3 - 4p_1^2p_2^3p_4 + 18p_1^3p_2p_3p_4 - 27p_1^4p_4^2 + 256p_0^3p_4^3) \\ &+p_0(-4p_2^3p_3^2 + 18p_1p_2p_3^3 + 16p_2^4p_4 - 80p_1p_2^2p_3p_4 - 6p_1^2p_3^2p_4 + 144p_1^2p_2p_4^2) \\ &+p_0^2(-27p_3^4 + 144p_2p_3^2p_4 - 128p_2^2p_4^2 - 192p_1p_3p_4^2) . \end{aligned} \tag{46}$$

We find that the discriminant of the characteristic polynomial is:

$$\Delta_4 = \frac{16gh^2T^2\beta_u}{L_I} k_{wx}^2 \left(k_{wx}^2 - k_{wy}^2\right) , \tag{47}$$

where $\beta_u = \beta^* q_x^2/h^2$ and:

$$T = L_I g \left[L_I g \left(k_{wx}^2 + k_{wy}^2\right)^2 + \beta_u \left(6k_{wx}^2k_{wy}^2 - 2k_{wx}^4\right)\right] + \beta_u^2 k_{wx}^4 . \tag{48}$$

As the coefficients of the characteristic polynomial $p(\omega)$ are all real, a positive discriminant indicates that either all the roots are real or all the roots are complex. A negative discriminant indicates that

there are two real and two complex roots. The complex roots come in pairs of complex conjugates. For this reason, if the discriminant is negative there exist an eigenvalue with a positive imaginary component. As the discriminant is negative for $k_{\mathrm{wx}} < k_{\mathrm{wy}}$ independently from the wave number, there exists always a region of growth. This implies that the model is ill-posed.

D Proof of Ill-posedness Due to Lack of Bed Slope Effect under Unisize Conditions

In this section we prove that the model based on the Shallow Water Equations without accounting for the effect of secondary flow in combination with the *Exner* (1920) equation to model bed elevation changes is ill-posed if the effect of the bed slope on the direction of the sediment transport is not taken into consideration.

The system of equations is composed of the first three and the fifth rows and columns of the system of equations in equation (24). Neglecting diffusive processes in the momentum equations and the effect of the bed slope, matrices $\mathbf{D_{x0}}$ and $\mathbf{D_{y0}}$ are equal to $\mathbb{0}$. The system of equations has 4 unknowns (h, q_{x}, q_{y}, and η). The unknowns are coupled meaning that a change in bed elevation influences the flow and vice versa. The celerity of perturbations associated with the flow variables (i.e., h, q_{x}, and q_{y}) are orders of magnitude larger than the celerity of perturbations in bed elevation if the Froude number is sufficiently small ($\mathrm{Fr} \lessapprox 0.7$ (*De Vries*, 1965, 1973; *Lyn and Altinakar*, 2002)). Under this condition we can decouple the system and consider steady flow to study the propagation of perturbations in bed elevation (i.e., quasi-steady flow assumption (*De Vries*, 1965; *Cao and Carling*, 2002; *Colombini and Stocchino*, 2005)). In this manner we reduce the number of unknowns to one (η), which means that there is only one eigenvalue (ω). We obtain ω equating to 0 the determinant of matrix:

$$\mathbf{R} = \begin{bmatrix} 0 & 0 & 0 & 0 \\ 0 & 0 & 0 & 0 \\ 0 & 0 & 0 & 0 \\ 0 & 0 & 0 & \omega \end{bmatrix} - \mathbf{M_0} \quad . \tag{49}$$

The growth rate (the imaginary part of ω) is:

$$\omega_{\mathrm{i}} = \frac{q_{\mathrm{b}} C_{\mathrm{f}} k_{\mathrm{wx}}^2}{k_{\mathrm{wx}}^2 w_2^2 + w_1^2} \left(w_3 + (n-1)\, k_{\mathrm{wy}}^4 \right) \ , \tag{50}$$

where w_1, w_2, and w_3 are second degree polynomials on k_{wy}:

$$w_1 = C_{\mathrm{f}} \left[\left(1 - 4\mathrm{Fr}^2 \right) k_{\mathrm{wx}}^2 + 2 k_{\mathrm{wy}}^2 \right] \ , \tag{51}$$

$$w_2 = b_1 + \left(1 - \mathrm{Fr}^2\right) k_{\mathrm{wx}}^2 + k_{\mathrm{wy}}^2 \ , \tag{52}$$

$$w_3 = -3\mathrm{Fr}^2 n k_{\mathrm{wx}}^4 - b_1 n k_{\mathrm{wx}}^2 + \left[n\left(2 - \mathrm{Fr}^2\right) - \left(2 + \mathrm{Fr}^2\right)\right] k_{\mathrm{wx}}^2 k_{\mathrm{wy}}^2 + b_1 \left(n - 3\right) k_{\mathrm{wy}}^2 \ , \tag{53}$$

where b_1 is:

$$b_1 = \frac{3 C_{\mathrm{f}}^2 \mathrm{Fr}^2}{h^2} \ . \tag{54}$$

Parameter n is the degree of non-linearity of the sediment transport relation (*Mosselman et al.*, 2008):

$$n = \frac{Q}{q_{\mathrm{b}}} \frac{\partial q_{\mathrm{b}}}{\partial Q} \ , \tag{55}$$

which is larger than 1. For instance, $n = 5$ in the relation developed by *Engelund and Hansen* (1967) and $n > 3$ in the one by *Meyer-Peter and Müller* (1948). In general $n > 3$ for the sediment transport relation to be physically realistic (*Mosselman*, 2005).

For k_{wy} tending to infinity, parameter w_3 becomes negligible with respect to $(n-1)k_{\mathrm{wy}}^4$. As all other terms in equation (50) are positive, for a large wave number the growth rate is positive which implies that the model is ill-posed.

E Well-Posed Domain under Mixed-Size Sediment Conditions

In this section we show that the Shallow Water Equations in combination with the active layer model (*Hirano*, 1971) used to account for mixed-size sediment morphodynamics may yield an ill-posed model depending on the closure relation used to account for the effect of the bed slope on the sediment transport direction.

We consider a model with two sediment size fractions. The system of equations is composed of the first three, the fifth and the sixth rows and columns of the full system of equations in equation (24). We neglect diffusive processes in the momentum equations. The system of equations has 5 unknowns (h, q_{x}, q_{y}, η, and M_{a1}). We consider that the Froude number is sufficiently small such that the quasi-steady approximation is valid (Appendix D) and we assume that the celerity associated with changes in the grain size distribution of the bed surface are of the same order of magnitude as the celerity of bed elevation changes (*Ribberink*, 1987; *Sieben*, 1997; *Stecca et al.*, 2016). Under these conditions it is valid to decouple the system and consider steady flow to study the propagation of perturbations in bed elevation and bed surface grain size distribution. In this manner we reduce the number of unknowns to two (η and M_{a1}), which means that there are two

angular frequencies to find. We obtain ω equating to 0 the determinant of matrix:

$$\mathbf{R} = \begin{bmatrix} 0 & 0 & 0 & 0 & 0 \\ 0 & 0 & 0 & 0 & 0 \\ 0 & 0 & 0 & 0 & 0 \\ 0 & 0 & 0 & \omega & 0 \\ 0 & 0 & 0 & 0 & \omega \end{bmatrix} - \mathbf{M_0} \quad . \tag{56}$$

We define a set of physically meaningful parameters useful to simplify the expression of the growth rate. Subscripts k and l refer to the grain size fraction while the subscript j refers to the direction (i.e., x and y). The parameters are a generalization of the parameters used by *Stecca et al.* (2014) and *Chavarrías et al.* (2018) to the x and y direction.

Parameter ψ_j $[-]$ represents the sediment transport intensity (e.g. *De Vries*, 1965; *Lyn and Altinakar*, 2002; *Stecca et al.*, 2014) and ranges between 0 (no sediment transport) and $\mathcal{O}(10^{-2})$ (high sediment discharge):

$$\psi_j = \frac{\partial q_{\mathrm{b}j}}{\partial q_j} \ . \tag{57}$$

Parameter $c_{jk} \in [0,1]$ $[-]$ represents the sediment transport intensity of fraction k relative to the total sediment transport intensity:

$$c_{jk} = \frac{1}{\psi_j} \frac{\partial q_{\mathrm{b}jk}}{\partial q_j} \ . \tag{58}$$

Parameter γ_{jk} $[-]$ represents the sediment transport intensity of fraction k relative to the fraction content of sediment of fraction k at the interface between the active layer and the substrate:

$$\gamma_{jk} = c_{jk} - f_k^{\mathrm{I}} \ , \tag{59}$$

Parameter χ_{jk} $[-]$ represents the nondimensional rate of change of the total sediment transport rate with respect to the change of volume of sediment of size fraction k in the active layer:

$$\chi_{jk} = \frac{1}{u_j} \frac{\partial q_{\mathrm{b}j}}{\partial M_{\mathrm{a}k}} \ . \tag{60}$$

Parameter $d_{jk,l}$ $[-]$ represents the nondimensional rate of change of the sediment transport rate of size fraction l with respect to the volume of sediment of size fraction k in the active layer:

$$d_{jk,l} = \frac{1}{u_j \chi_{jk}} \frac{\partial q_{\mathrm{b}jl}}{\partial M_{\mathrm{a}k}} \ . \tag{61}$$

Parameter $\mu_{jk,l}$ $[-]$ represents the rate of change of the sediment transport rate with respect to the volume of sediment in the active layer relative to the fraction content of sediment of fraction

k at the interface between the active layer and the substrate:

$$\mu_{jk,l} = d_{jk,l} - f_k^{\mathrm{I}} \ . \tag{62}$$

Parameter $R_j < 0$ [m^2/s] represents the effect of the bed slope on the direction of the sediment transport rate:

$$R_j = \frac{\partial q_{\mathrm{b}j}}{\partial s_j} \ , \tag{63}$$

where $s_j = \partial\eta/\partial j$. Parameter r_{jk} [$-$] represents the effect of the bed slope on the direction of the sediment transport rate of fraction k relative to the total effect:

$$r_{jk} = \frac{1}{R_j}\frac{\partial q_{\mathrm{b}jk}}{\partial s_j} \ . \tag{64}$$

Parameter l_{jk} [$-$] represents the effect of the bed slope on the direction of the sediment transport rate of fraction k relative to the fraction content of sediment at the interface between the active layer and the substrate:

$$l_{jk} = r_{jk} - f_k^{\mathrm{I}} \ . \tag{65}$$

The largest of the two growth rates (i.e., the largest imaginary part of the two eigenvalues ω of the system) is:

$$\omega_{\mathrm{i}} = \frac{1}{2}\left(\frac{\sqrt{2}}{2}\sqrt{f_1} - \sqrt{f_2}\right) \ , \tag{66}$$

where:

$$f_1 = \sqrt{m_1^2 + m_2} - m_1 \ , \tag{67}$$

and:

$$f_2 = R_{\mathrm{y}}^2 k_{\mathrm{wy}}^4 \ . \tag{68}$$

When parameter f_1 is larger than $2f_2$, $\omega_{\mathrm{i}} > 0$ and perturbations grow. Parameter f_1 becomes large with respect to f_2 when parameter m_2 becomes large with respect to m_1 where:

$$m_1 = k_{\mathrm{wx}}^2 u^2 a_3 - f_2 \ , \tag{69}$$

and:

$$m_2 = 4k_{\mathrm{wx}}^2 u^2 f_2 o^2 \ . \tag{70}$$

Focusing on the bed slope effect, for a given value of f_2 (i.e., a given value of R_{y}), parameter m_2 becomes large with respect to m_1 when parameter o becomes large, where:

$$o = a_1 + 2\chi_{\mathrm{x}1}\left(r_{\mathrm{y}1} - d_{\mathrm{x}1,1}\right) \ . \tag{71}$$

Thus, the growth rate of perturbations is prone to be positive when the absolute value of $r_{y1} - d_{x1,1}$ increases. The parameters a_m for $m = 1, 2, 3$ are:

$$a_1 = e_x + e_y + \chi_{x1}\mu_{x1,1} \ , \tag{72}$$

$$a_2 = \gamma_{x1}e_x + \gamma_{y1}e_y - \mu_{x1,1}e_x - \mu_{x1,1}e_y \ , \tag{73}$$

$$a_3 = a_1^2 + 4\chi_{x1}a_2 \ . \tag{74}$$

The parameters e_j for $j = x, y$ are:

$$e_x = \psi_x \frac{k_{wx}^2}{\left(1 - \mathrm{Fr}^2\right) k_{wx}^2 + k_{wy}^2} \ , \tag{75}$$

$$e_y = \psi_y \frac{k_{wy}^2}{\left(1 - \mathrm{Fr}^2\right) k_{wx}^2 + k_{wy}^2} \ . \tag{76}$$

We compute the limit of the growth rate (equation (66)) for k_{wx} and k_{wy} tending to infinity:

$$\omega_i^{\lim} = \alpha_1 \left(r_{y1} - d_{x1,1}\right)^2 + \alpha_2 \left(r_{y1} - d_{x1,1}\right) + \alpha_3 \ , \tag{77}$$

where:

$$\alpha_1 = \frac{-u^2\chi_{x1}}{R_y}\chi_{x1} \ , \quad \alpha_2 = \frac{-u^2\chi_{x1}}{R_y}a_1^{\lim} \ , \quad \alpha_3 = \frac{u^2\chi_{x1}}{R_y}a_2^{\lim} \ , \tag{78}$$

where the superscript lim indicates that these are the limit values and:

$$e_x^{\lim} = \frac{\psi_x}{2 - \mathrm{Fr}^2} \ , \tag{79}$$

$$e_y^{\lim} = \frac{\psi_y}{2 - \mathrm{Fr}^2} \ . \tag{80}$$

As $R_y < 0$ and $\chi_{x1} > 0$, the mathematical character of the system of equations is given by the sign of the second degree polynomial with variable $(r_{y1} - d_{x1,1})$. The fact that $\alpha_1 > 0$ (the factor of the squared term) indicates that the model is well-posed when $r_{y1}^- < r_{y1} < r_{y1}^+$ where:

$$r_{y1}^{\pm} = \frac{1}{2\chi_{x1}} \left(-a_1^{\lim} \pm \sqrt{a_1^{\lim^2} + 4\chi_{x1}a_2^{\lim}} \right) + d_{x1,1} \ . \tag{81}$$

References

Armanini, A., and G. di Silvio (1988), A one-dimensional model for the transport of a sediment mixture in non-equilibrium conditions, *J. Hydraul. Res.*, *26*(3), 275–292, doi:10.1080/

00221688809499212.

Ashida, K., and M. Michiue (1971), An investigation of river bed degradation downstream of a dam, in *Proc. of the 14th IAHR World Congress, 29 August–3 Septemeber, Paris, France*, vol. 3, pp. 247–255.

Baar, A. W., J. de Smit, W. S. J. Uijttewaal, and M. G. Kleinhans (2018), Sediment transport of fine sand to fine gravel on transverse bed slopes in rotating annular flume experiments, *Water Resour. Res.*, *54*, doi:10.1002/2017WR020604.

Balmforth, N. J., and S. Mandre (2004), Dynamics of roll waves, *J. Fluid Mech.*, *514*, 1–33, doi:10.1017/S0022112004009930.

Balmforth, N. J., and A. Vakil (2012), Cyclic steps and roll waves in shallow water flow over an erodible bed, *J. Fluid Mech.*, *695*, 35–62, doi:10.1017/jfm.2011.555.

Banks, J., J. Brooks, G. Cairns, G. Davis, and P. Stacey (1992), On Devaney's definition of chaos, *The American Mathematical Monthly*, *99*(4), 332–334, doi:10.2307/2324899.

Barker, B., M. A. Johnson, P. Noble, L. M. Rodrigues, and K. Zumbrun (2017a), Note on the stability of viscous roll waves, *C. R. Mec.*, *345*(2), 125–129, doi:10.1016/j.crme.2016.11.001.

Barker, B., M. A. Johnson, P. Noble, L. M. Rodrigues, and K. Zumbrun (2017b), Stability of viscous St. Venant roll waves: From onset to infinite Froude number limit, *J. Nonlinear Sci.*, *27*(1), 285–342, doi:10.1007/s00332-016-9333-6.

Barker, T., and J. M. N. T. Gray (2017), Partial regularisation of the incompressible μ-rheology for granular flow, *J. Fluid Mech.*, *828*, 5–32, doi:10.1017/jfm.2017.428.

Barker, T., D. G. Schaeffer, P. Bohorquez, and J. M. N. T. Gray (2015), Well-posed and ill-posed behaviour of the μ-rheology for granular flow, *J. Fluid Mech.*, *779*, 794–818, doi:10.1017/jfm.2015.412.

Beeler, M., R. W. Gosper, and R. C. Schroeppel (1972), HAKMEM, *MIT AI Memo 239*, Artificial Intelligence Laboratory, Massachusetts Institute of Technology, Cambridge, MA, United States, 107 pp.

Begnudelli, L., A. Valiani, and B. F. Sanders (2010), A balanced treatment of secondary currents, turbulence and dispersion in a depth-integrated hydrodynamic and bed deformation model for channel bends, *Adv. Water Resour.*, *33*(1), 17–33, doi:10.1016/j.advwatres.2009.10.004.

Bell, R. G., and A. J. Sutherland (1983), Nonequilibrium bedload transport by steady flows, *J. Hydraul. Eng.*, *109*(3), doi:10.1061/(ASCE)0733-9429(1983)109:3(351).

van Bendegom, L. (1947), Eenige beschouwingen over riviermorphofogie en rivierverbetering, *De Ingenieur*, *59*(4), 1–11, (in Dutch).

Blanckaert, K. (2009), Saturation of curvature-induced secondary flow, energy losses, and turbulence in sharp open-channel bends: Laboratory experiments, analysis, and modeling, *J. Geophys. Res., Earth Surface*, *114*, F03015, doi:10.1029/2008JF001137.

Blanckaert, K., and H. J. de Vriend (2003), Nonlinear modeling of mean flow redistribution in curved open channels, *Water Resour. Res.*, *39*(12), doi:10.1029/2003WR002068.

Blanckaert, K., and W. H. Graf (2004), Momentum transport in sharp open-channel bends, *J. Hydraul. Eng.*, *130*(3), 186–198, doi:10.1061/(ASCE)0733-9429(2004)130:3(186).

Blanckaert, K., and H. J. de Vriend (2004), Secondary flow in sharp open-channel bends, *J. Fluid Mech.*, *498*, 353–380, doi:10.1017/S0022112003006979.

Blom, A. (2008), Different approaches to handling vertical and streamwise sorting in modeling river morphodynamics, *Water Resour. Res.*, *44*(3), W03415, doi:10.1029/2006WR005474.

Blom, A., E. Viparelli, and V. Chavarrías (2016), The graded alluvial river: Profile concavity and downstream fining, *Geophys. Res. Lett.*, *43*, 6285–6293, doi:10.1002/2016GL068898.

Blom, A., L. Arkesteijn, V. Chavarrías, and E. Viparelli (2017), The equilibrium alluvial river under variable flow and its channel-forming discharge, *J. Geophys. Res., Earth Surface*, *122*, doi:10.1002/2017JF004213.

Booij, R., and J. G. S. Pennekamp (1983), Simulation of main flow and secondary flow in a curved open channel, *Tech. Rep. 10-83*, Laboratory of Fluid Mechanics, Faculty of Civil Engineering and Geosciences, Delft University of Technology, Delft, the Netherlands, 62 pp.

Booij, R., and J. G. S. Pennekamp (1984), Measurements of the rate of adjustement of the secondary flow in a curved open channel with varying discharge, *Tech. Rep. 15-84*, Laboratory of Fluid Mechanics, Faculty of Civil Engineering and Geosciences, Delft University of Technology, Delft, the Netherlands, 44 pp.

Bradshaw, P. (1987), Turbulent secondary flows, *Annu. Rev. Fluid Mech.*, *19*(1), 53–74, doi:10.1146/annurev.fl.19.010187.000413.

Bressan, A. (2011), Hyperbolic conservation laws, in *Mathematics of Complexity and Dynamical Systems*, edited by R. A. Meyers, chap. 44, pp. 729–739, Springer, New York, NY, United States, doi:10.1007/978-1-4614-1806-1_44.

Brundrett, E., and W. D. Baines (1964), The production and diffusion of vorticity in duct flow, *J. Fluid Mech.*, *19*(3), 375–394, doi:10.1017/S0022112064000799.

Callander, R. A. (1969), Instability and river channels, *J. Fluid Mech.*, *36*(3), 465–480, doi:10.1017/S0022112069001765.

Cao, Z., and P. A. Carling (2002), Mathematical modelling of alluvial rivers: Reality and myth. Part 1: General review, *Proceedings of the Institution of Civil Engineers Water & Maritime Engineering*, *154*(3), 207–219.

Castro, M. J., E. D. Fernández-Nieto, A. M. Ferreiro, J. A. García-Rodríguez, and C. Parés (2009), High order extensions of Roe schemes for two-dimensional nonconservative hyperbolic systems, *J. Sci. Comput.*, *39*(1), 67–114, doi:10.1007/s10915-008-9250-4.

Chavarrías, V., G. Stecca, and A. Blom (2018), Ill-posedness in modelling mixed-sediment river morphodynamics, *Adv. Water Resour.*, *114*, 219–235, doi:10.1016/j.advwatres.2018.02.011.

Colombini, M. (1993), Turbulence-driven secondary flows and formation of sand ridges, *J. Fluid Mech.*, *254*, 701–719, doi:10.1017/S0022112093002319.

Colombini, M., and A. Stocchino (2005), Coupling or decoupling bed and flow dynamics: Fast and slow sediment waves at high froude numbers, *Phys. Fluids*, *17*(3), 036602, doi:10.1063/1.1848731.

Colombini, M., and A. Stocchino (2011), Ripple and dune formation in rivers, *J. Fluid Mech.*, *673*, 121–131, doi:10.1017/S0022112011000048.

Colombini, M., and A. Stocchino (2012), Three-dimensional river bed forms, *J. Fluid Mech.*, *695*, 63–80, doi:10.1017/jfm.2011.556.

Colombini, M., G. Seminara, and M. Tubino (1987), Finite-amplitude alternate bars, *J. Fluid Mech.*, *181*, 213–232, doi:10.1017/S0022112087002064.

Cordier, S., M. Le, and T. M. de Luna (2011), Bedload transport in shallow water models: Why splitting (may) fail, how hyperbolicity (can) help, *Adv. Water Resour.*, *34*(8), 980–989, doi:10.1016/j.advwatres.2011.05.002.

Courant, R., and D. Hilbert (1989), *Methods of Mathematical Physics, Volume 2: Differential Equations*, 852 pp., John Wiley & Sons, New York, NY, United States.

Dafermos, C. M. (2010), *Hyperbolic Conservation Laws in Continuum Physics*, no. 325 in Grundlehren der mathematischen Wissenschaften, 3 ed., 708 pp., Springer Berlin, Heidelberg, Germany.

Dafermos, C. M. (2016), Introduction to the theory of hyperbolic conservation laws, in *Handbook of Numerical Methods for Hyperbolic Problems*, *Handbook of Numerical Analysis*, vol. 17, edited by R. Abgrall and C.-W. Shu, chap. 1, pp. 1–18, Elsevier, Amsterdam, the Netherlands, doi:10.1016/bs.hna.2016.08.003.

Deigaard, R., and J. Fredsøe (1978), Longitudinal grain sorting by current in alluvial streams, *Nord. Hydrol.*, *9*(1), 7–16, doi:10.2166/nh.1978.002.

Devaney, R. L. (1989), *An Introduction to Chaotic Dynamical Systems*, 336 pp., Addison-Wesley, Boston, MA, United States.

Dietrich, W. E., and J. D. Smith (1984), Bed load transport in a river meander, *Water Resour. Res.*, *20*(10), 1355–1380, doi:10.1029/WR020i010p01355.

Einstein, H. A. (1950), The bed-load function for sediment transportation in open channel flows, *Tech. Bull. 1026*, US Department of Agriculture, Soil Conservation Service, Washington, DC, United States, 70 pp.

Einstein, H. A., and H. Li (1958), Secondary currents in straight channels, *Eos, Transactions American Geophysical Union*, *39*(6), 1085–1088, doi:10.1029/TR039i006p01085.

Elder, J. W. (1959), The dispersion of marked fluid in turbulent shear flow, *J. Fluid Mech.*, *5*(4), 544–560, doi:10.1017/S0022112059000374.

Engelund, F. (1974), Flow and bed topography in channel bends, *J. Hydraulics Div.*, *100*(11), 1631–1648.

Engelund, F. (1975), Instability of flow in a curved alluvial channel, *J. Fluid Mech.*, *72*(1), 145–160, doi:10.1017/S002211207500300X.

Engelund, F., and E. Hansen (1967), Monograph on sediment transport in alluvial streams, *Tech. Rep.*, Hydraulics Laboratory, Technical University of Denmark, Copenhagen, Denmark, 63 pp.

Engelund, F., and O. Skovgaard (1973), On the origin of meandering and braiding in alluvial streams, *J. Fluid Mech.*, *57*(2), 289–302, doi:10.1017/S0022112073001163.

Erdogan, M. E., and P. C. Chatwin (1967), The effects of curvature and buoyancy on the laminar dispersion of solute in a horizontal tube, *J. Fluid Mech.*, *29*(3), 465–484, doi:10.1017/S0022112067000977.

Exner, F. M. (1920), Zur Physik der Dünen, *Akad. Wiss. Wien Math. Naturwiss*, *129(2a)*, 929–952, (in German).

Falconer, R. A. (1980), Modelling of planform influence on circulation in harbours, in *Proc. 17th Int. Conference on Coastal Eng., 23-28 March, Sydney, Australia*, pp. 2726–2744, doi:10.1061/9780872622647.164.

Fischer, H. B. (1967), The mechanics of dispersion in natural streams, *J. Hydraulics Div.*, *96*(6), 187–216.

1086 Fischer, H. B. (1969), The effect of bends on dispersion in streams, *Water Resour. Res.*, *5*(2),
1087 496–506, doi:10.1029/WR005i002p00496.

1088 Fischer, H. B. (1973), Longitudinal dispersion and turbulent mixing in open-channel flow, *Annu.*
1089 *Rev. Fluid Mech.*, *5*(1), 59–78, doi:10.1146/annurev.fl.05.010173.000423.

1090 Flokstra, C. (1977), The closure problem for depth-averaged 2-D flow, in *Proc. 18th IAHR World*
1091 *Congress, 15–19 August, Baden-Baden, Germany.*

1092 Fowler, A. C. (1997), *Mathematical Models in the Applied Sciences*, Cambridge Texts in Applied
1093 Mathematics, 424 pp., Cambridge University Press, Cambridge, United Kingdom.

1094 Francalanci, S., and L. Solari (2007), Gravitational effects on bed load transport at low
1095 Shields stress: Experimental observations, *Water Resour. Res.*, *43*(3), W03424, doi:10.1029/
1096 2005WR004715.

1097 Francalanci, S., and L. Solari (2008), Bed-load transport equation on arbitrarily sloping beds, *J.*
1098 *Hydraul. Eng.*, *134*(1), 110–115, doi:10.1061/(ASCE)0733-9429(2008)134:1(110).

1099 Fredsøe, J. (1978), Meandering and braiding of rivers, *J. Fluid Mech.*, *84*(4), 609–624, doi:10.1017/
1100 S0022112078000373.

1101 Garegnani, G., G. Rosatti, and L. Bonaventura (2011), Free surface flows over mobile bed: Mathe-
1102 matical analysis and numerical modeling of coupled and decoupled approaches, *Commun. Appl.*
1103 *Ind. Math.*, *2*(1), doi:10.1685/journal.caim.371.

1104 Garegnani, G., G. Rosatti, and L. Bonaventura (2013), On the range of validity of the Exner-
1105 based models for mobile-bed river flow simulations, *J. Hydraul. Res.*, *51*(4), 380–391, doi:10.
1106 1080/00221686.2013.791647.

1107 Gavrilakis, S. (1992), Numerical simulation of low-Reynolds-number turbulent flow through a
1108 straight square duct, *J. Fluid Mech.*, *244*, 101–129, doi:10.1017/S0022112092002982.

1109 Gessner, F. B., and J. B. Jones (1965), On some aspects of fully-developed turbulent flow in
1110 rectangular channels, *J. Fluid Mech.*, *23*(4), 689–713, doi:10.1017/S0022112065001635.

1111 Giri, S., and Y. Shimizu (2006), Numerical computation of sand dune migration with free surface
1112 flow, *Water Resour. Res.*, *42*(10), W10422, doi:10.1029/2005WR004588.

1113 Hadamard, J. S. (1923), *Lectures on Cauchy's problem in linear partial differential equations*, 316
1114 pp., Yale University Press, New Haven, CT, United States.

1115 Hirano, M. (1971), River bed degradation with armoring, *Proc. Jpn. Soc. Civ. Eng.*, *195*, 55–65,
1116 doi:10.2208/jscej1969.1971.195_55.

1117 Hoey, T. B., and R. I. Ferguson (1994), Numerical simulation of downstream fining by selective
1118 transport in gravel bed rivers: Model development and illustration, *Water Resour. Res.*, *30*(7),
1119 2251–2260, doi:10.1029/94WR00556.

1120 Holley, E. R. (1971), Transverse mixing in rivers, *Tech. Rep. S132*, Delft Hydraulics Laboratory,
1121 Delft, the Netherlands, 96 pp.

1122 Ikeda, S., and T. Nishimura (1985), Bed topography in bends of sand-silt rivers, *J. Hydraul. Eng.*,
1123 *111*(11), 1397–1410, doi:10.1061/(ASCE)0733-9429(1985)111:11(1397).

1124 Ikeda, S., and T. Nishimura (1986), Flow and bed profile in meandering sand-silt rivers, *J. Hydraul.*
1125 *Eng.*, *112*(7), 562–579, doi:10.1061/(ASCE)0733-9429(1986)112:7(562).

1126 Ikeda, S., G. Parker, and K. Sawai (1981), Bend theory of river meanders. Part 1. Linear develop-
1127 ment, *J. Fluid Mech.*, *112*, 363–377, doi:10.1017/S0022112081000451.

1128 Jagers, B. (2003), Modelling planform changes of braided rivers, Ph.D. thesis, University of Twente,
1129 Enschede, the Netherlands.

1130 Jain, S. C. (1992), Note on lag in bedload discharge, *J. Hydraul. Eng.*, *118*(6), 904–917, doi:
1131 10.1061/(ASCE)0733-9429(1992)118:6(904).

1132 Javernick, L., D. M. Hicks, R. Measures, B. Caruso, and J. Brasington (2016), Numerical modelling
1133 of braided rivers with structure-from-motion-derived terrain models, *River Res. Appl.*, *32*(5),
1134 1071–1081, doi:10.1002/rra.2918.

1135 Javernick, L., M. Redolfi, and W. Bertoldi (2018), Evaluation of a numerical model's ability to
1136 predict bed load transport observed in braided river experiments, *Adv. Water Resour.*, *115*,
1137 207–218, doi:10.1016/j.advwatres.2018.03.012.

1138 Jeffreys, H. (1925), The flow of water in an inclined channel of rectangular section, *The London,*
1139 *Edinburgh, and Dublin Philosophical Magazine and Journal of Science*, *49*(293), 793–807, doi:
1140 10.1080/14786442508634662.

1141 Johannesson, H., and G. Parker (1989), Secondary flow in mildly sinuous channel, *J. Hydraul.*
1142 *Eng.*, *115*(3), 289–308, doi:10.1061/(ASCE)0733-9429(1989)115:3(289).

1143 Jop, P., Y. Forterre, and O. Pouliquen (2005), Crucial role of sidewalls in granular surface flows:
1144 Consequences for the rheology, *J. Fluid Mech.*, *541*, 167–192, doi:10.1017/S0022112005005987.

1145 Jop, P., Y. Forterre, and O. Pouliquen (2006), A constitutive law for dense granular flows, *Nature*,
1146 *441*, 727–730, doi:10.1038/nature04801.

1147 Joseph, D., and J. Saut (1990), Short-wave instabilities and ill-posed initial-value problems, *Theor.*
1148 *Comput. Fluid Mech.*, *1*(4), 191–227, doi:10.1007/BF00418002.

Kabanikhin, S. I. (2008), Definitions and examples of inverse and ill-posed problems, *J. Inv. Ill-Posed Problems*, *16*, 317–357, doi:10.1515/JIIP.2008.019.

Kalkwijk, J. P. T., and R. Booij (1986), Adaptation of secondary flow in nearly-horizontal flow, *J. Hydraul. Res.*, *24*(1), 19–37, doi:10.1080/00221688609499330.

Kalkwijk, J. P. T., and H. J. de Vriend (1980), Computation of the flow in shallow river bends, *J. Hydraul. Res.*, *18*(4), 327–342, doi:10.1080/00221688009499539.

Kitanidis, P. K., and J. F. Kennedy (1984), Secondary current and river-meander formation, *J. Fluid Mech.*, *144*, 217–229, doi:10.1017/S0022112084001580.

Knowles, J. K., and E. Sternberg (1975), On the ellipticity of the equations of nonlinear elastostatics for a special material, *J. Elast.*, *5*(3), 341–361, doi:10.1007/BF00126996.

Knowles, J. K., and E. Sternberg (1976), On the failure of ellipticity of the equations for finite elastostatic plane strain, *Arch. Ration. Mech. Anal.*, *63*(4), 321–336, doi:10.1007/BF00279991.

Koch, F. G., and C. Flokstra (1981), Bed level computations for curved alluvial channels, in *Proc. 19th IAHR World Congress, 2–7 February, New Delhi, India.*

Kyong, O. B., and W. S. Il (2016), On the methods for determining the transverse dispersion coefficient in river mixing, *Adv. Water Resour.*, *90*, 1–9, doi:10.1016/j.advwatres.2016.01.009.

Lanzoni, S., and M. Tubino (1999), Grain sorting and bar instability, *J. Fluid Mech.*, *393*, 149–174, doi:10.1017/S0022112099005583.

Lax, P. D. (1980), On the notion of hyperbolicity, *Commun. Pure Appl. Math.*, *33*, 395–397.

Legleiter, C. J., and P. C. Kyriakidis (2006), Forward and inverse transformations between Cartesian and channel-fitted coordinate systems for meandering rivers, *Math. Geol.*, *38*(8), 927–958, doi:10.1007/s11004-006-9056-6.

Lesser, G., J. Roelvink, J. van Kester, and G. Stelling (2004), Development and validation of a three-dimensional morphological model, *Coastal Eng.*, *51*, 883–915, doi:10.1016/j.coastaleng.2004.07.014.

LeVeque, R. J. (2004), *Finite Volume Methods for Hyperbolic Problems*, no. 31 in Cambridge Texts in Applied Mathematics, Cambridge University Press, Cambridge, United Kingdom, doi:10.1017/CBO9780511791253.

Lien, H. C., T. Y. Hsieh, J. C. Yang, and K. C. Yeh (1999), Bend-flow simulation using 2D depth-averaged model, *J. Hydraul. Eng.*, *125*(10), 1097–1108, doi:10.1061/(ASCE)0733-9429(1999)125:10(1097).

Lorenz, E. N. (1963), Deterministic nonperiodic flow, *J. Atmos. Sci.*, *20*(2), 130–141, doi:10.1175/1520-0469(1963)020⟨0130:DNF⟩2.0.CO;2.

Lyn, D. A., and M. Altinakar (2002), St. Venant-Exner equations for near-critical and transcritical flows, *J. Hydraul. Eng.*, *128*(6), 579–587, doi:10.1061/(ASCE)0733-9429(2002)128:6(579).

Meyer-Peter, E., and R. Müller (1948), Formulas for bed-load transport, in *Proc. 2nd IAHR World Congress, 6–9 June, Stockholm, Sweden*, pp. 39–64.

Mosselman, E. (2005), Basic equations for sediment transport in CFD for fluvial morphodynamics, in *Computational Fluid Dynamics: Applications in Environmental Hydraulics*, edited by P. D. Bates, S. N. Lane, and R. I. Ferguson, chap. 4, pp. 71–89, John Wiley & Sons, Chichester, United Kingdom.

Mosselman, E., K. Sloff, and S. van Vuren (2008), Different sediment mixtures at constant flow conditions can produce the same celerity of bed disturbances, in *River Flow 2008, Proc. Int. Conference on Fluvial Hydr., 3-5 September, Cesme, Izmir, Turkey*, vol. 2, edited by M. Altinakar, M. A. Kokpinar, İsmail Aydin, Şevket Cokgor, and S. Kirgoz, pp. 1373–1377, Kubaba Congress Department and Travel Services, Ankara, Turkey.

Murray, A. B. (2007), Reducing model complexity for explanation and prediction, *Geomorphology*, *90*(3-4), 178–191, doi:10.1016/j.geomorph.2006.10.020.

Murray, A. B., and C. Paola (1994), A cellular model of braided rivers, *Nature*, *371*(54), 54–57, doi:10.1038/371054a0.

Murray, A. B., and C. Paola (1997), Properties of a cellular braided-stream model, *Earth Surf. Process. Landf.*, *22*(11), 1001–1025, doi:10.1002/(SICI)1096-9837(199711)22:11⟨1001::AID-ESP798⟩3.0.CO;2-O.

Nezu, I., and H. Nakagawa (1984), Cellular secondary currents in straight conduit, *J. Hydraul. Eng.*, *110*(2), 173–193, doi:10.1061/(ASCE)0733-9429(1984)110:2(173).

Nikuradse, J. (1930), Untersuchungen über turbulente strömungen in nicht kreisförmigen rohren, *Ingenieur-Archiv*, *1*(3), 306–332, doi:10.1007/BF02079937, (in German).

Olesen, K. W. (1982), Influence of secondary flow on meandering rivers, *Tech. Rep. 1-82*, Laboratory of Fluid Mechanics, Faculty of Civil Engineering and Geosciences, Delft University of Technology, Delft, the Netherlands, 67 pp.

Ottevanger, W., K. Blanckaert, W. S. J. Uijttewaal, and H. J. de Vriend (2013), Meander dynamics: A reduced-order nonlinear model without curvature restrictions for flow and bed morphology, *J. Geophys. Res., Earth Surface*, *118*(2), 1118–1131, doi:10.1002/jgrf.20080.

Paola, C. (2000), Quantitative models of sedimentary basin filling, *Sedimentology*, *47*, 121–178, doi:10.1046/j.1365-3091.2000.00006.x.

Paola, C., and M. Leeder (2011), Environmental dynamics: Simplicity versus complexity, *Nature*, *469*, 38–39, doi:10.1038/469038a.

Paola, C., P. L. Heller, and C. L. Angevine (1992), The large-scale dynamics of grain-size variation in alluvial basins, 1: Theory, *Basin Res.*, *4*(2), 73–90, doi:10.1111/j.1365-2117.1992.tb00145.x.

Parker, G. (1976), On the cause and characteristic scales of meandering and braiding in rivers, *J. Fluid Mech.*, *76*(3), 457–480, doi:10.1017/S0022112076000748.

Parker, G. (1978), Self-formed straight rivers with equilibrium banks and mobile bed. Part 1. The sand-silt river, *J. Fluid Mech.*, *89*(1), 109–125, doi:10.1017/S0022112078002499.

Parker, G. (1991), Selective sorting and abrasion of river gravel. I: Theory, *J. Hydraul. Eng.*, *117*(2), 131–147, doi:10.1061/(ASCE)0733-9429(1991)117:2(131).

Parker, G., and E. D. Andrews (1985), Sorting of bed load sediment by flow in meander bends, *Water Resour. Res.*, *21*(9), 1361–1373, doi:10.1029/WR021i009p01361.

Parker, G., and A. J. Sutherland (1990), Fluvial armor, *J. Hydraul. Res.*, *28*(5), 529–544, doi:10.1080/00221689009499044.

Parker, G., C. Paola, and S. Leclair (2000), Probabilistic Exner sediment continuity equation for mixtures with no active layer, *J. Hydraul. Eng.*, *126*(11), 818–826, doi:10.1061/(ASCE)0733-9429(2000)126:11(818).

Parker, G., G. Seminara, and L. Solari (2003), Bed load at low Shields stress on arbitrarily sloping beds: Alternative entrainment formulation, *Water Resour. Res.*, *39*(7), 1183, doi:10.1029/2001WR001253.

Phillips, B. C., and A. J. Sutherland (1989), Spatial lag effects in bed load sediment transport, *J. Hydraul. Res.*, *27*(1), 115–133, doi:10.1080/00221688909499247.

van Prooijen, B. C., and W. S. J. Uijttewaal (2002), A linear approach for the evolution of coherent structures in shallow mixing layers, *Phys. Fluids*, *14*(12), 4105–4114, doi:10.1063/1.1514660.

Qian, H., Z. Cao, H. Liu, and G. Pender (2016), Numerical modelling of alternate bar formation, development and sediment sorting in straight channels, *Earth Surf. Process. Landf.*, *42*(7), 555–574, doi:10.1002/esp.3988.

Ribberink, J. S. (1987), Mathematical modelling of one-dimensional morphological changes in rivers with non-uniform sediment, Ph.D. thesis, Delft University of Technology, Delft, the Netherlands.

Rodrigues, L., and K. Zumbrun (2016), Periodic-coefficient damping estimates, and stability of large-amplitude roll waves in inclined thin film flow, *SIAM J. Math. Anal.*, *48*(1), 268–280, doi:10.1137/15M1016242.

Rozovskii, I. L. (1957), *Flow of water in bends in open channels*, 233 pp., Academy of Sciences of the Ukrainian SSR, (in English translated by Y. Prushansky in 1961).

Saint-Venant, A. J. C. B. (1871), Théorie du mouvement non permanent des eaux, avec application aux crues des rivières et à l'introduction des marées dans leur lit, *Comptes Rendus des séances de l'Académie des Sciences*, *73*, 237–240, (in French).

Schielen, R., A. Doelman, and H. E. de Swart (1993), On the nonlinear dynamics of free bars in straight channels, *J. Fluid Mech.*, *252*, 325–356, doi:10.1017/S0022112093003787.

Seminara, G. (2006), Meanders, *J. Fluid Mech.*, *554*, 271–297, doi:10.1017/S0022112006008925.

Seminara, G., and M. Tubino (1989), Alternate bars and meandering, in *River Meandering*, edited by S. Ikeda and G. Parker, chap. 10, pp. 267–320, AGU, Washington, DC, United States, doi:10.1029/WM012p0267.

Seminara, G., L. Solari, and G. Parker (2002), Bed load at low Shields stress on arbitrarily sloping beds: Failure of the Bagnold hypothesis, *Water Resour. Res.*, *38*(11), 1249, doi:10.1029/2001WR000681.

Shields, A. (1936), Anwendung der Ähnlichkeitsmechanik und Turbulenzforschung auf die Geschiebebewegung, Ph.D. thesis, Versuchsanstalt für Wasserbau und Schiffbau, 26, Berlin, Germany, (in German).

Shimizu, Y., S. Giri, S. Yamaguchi, and J. Nelson (2009), Numerical simulation of dune-flat bed transition and stage-discharge relationship with hysteresis effect, *Water Resour. Res.*, *45*(4), W04429, doi:10.1029/2008WR006830.

Sieben, J. (1997), Modelling of hydraulics and morphology in mountain rivers, Ph.D. thesis, Delft University of Technology, Delft, the Netherlands.

Simons, D. B., and M. L. Albertson (1963), Uniform water conveyance channels in alluvial materials, *Transaction ASCE*, *128*, 65–105.

Siviglia, A., G. Stecca, and A. Blom (2017), Modeling of mixed-sediment morphodynamics in gravel bed rivers using the active layer approach: Insights from mathematical and numerical analysis, in *Gravel-Bed Rivers: Process and Disasters*, edited by D. Tsutsumi and J. Laronne, chap. 26, pp. 703–728, Wiley-Blackwell, Hoboken, NJ, United States, doi:10.1002/9781118971437.ch26.

Stecca, G., A. Siviglia, and A. Blom (2014), Mathematical analysis of the Saint-Venant-Hirano model for mixed-sediment morphodynamics, *Water Resour. Res.*, *50*, 7563–7589, doi:10.1002/2014WR015251.

Stecca, G., A. Siviglia, and A. Blom (2016), An accurate numerical solution to the Saint-Venant-Hirano model for mixed-sediment morphodynamics in rivers, *Adv. Water Resour.*, *93, Part A*, 39–61, doi:10.1016/j.advwatres.2015.05.022.

Strikwerda, J. (2004), *Finite Difference Schemes and Partial Differential Equations*, 2 ed., 427 pp., Society for Industrial and Applied Mathematics, Philadelphia, PA, United States, doi:10.1137/1.9780898717938.

Talmon, A., N. Struiksma, and M. V. Mierlo (1995), Laboratory measurements of the direction of sediment transport on transverse alluvial-bed slopes, *J. Hydraul. Res.*, *33*(4), doi:10.1080/00221689509498657.

Talstra, H. (2011), Large-scale turbulence structures in shallow separating flows, Ph.D. thesis, Delft University of Technology, Delft, the Netherlands.

Toro, E. F. (2009), *Riemann Solvers and Numerical Methods for Fluid Dynamics*, 3 ed., 724 pp., Springer-Verlag Berlin, Heidelberg, Germany, doi:10.1007/b79761.

Toro-Escobar, C. M., C. Paola, and G. Parker (1996), Transfer function for the deposition of poorly sorted gravel in response to streambed aggradation, *J. Hydraul. Res.*, *34*(1), 35–53, doi:10.1080/00221689609498763.

Veprek, R. G., S. Steiger, and B. Witzigmann (2007), Ellipticity and the spurious solution problem of k-p envelope equations, *Phys. Rev. B*, *76*, 165320, doi:10.1103/PhysRevB.76.165320.

Vreugdenhil, C. B. (1994), *Numerical Methods for Shallow-Water Flow*, 262 pp., Springer, Dordrecht, the Netherlands, doi:10.1007/978-94-015-8354-1.

de Vriend, H. J. (1977), A mathematical model of steady flow in curved shallow channels, *J. Hydraul. Res.*, *15*(1), 37–54, doi:10.1080/00221687709499748.

de Vriend, H. J. (1981), Steady flow in shallow channel bends, Ph.D. thesis, Delft University of Technology, Delft, the Netherlands.

de Vries, M. (1965), Considerations about non-steady bed load transport in open channels, *Tech. Rep. 36*, Delft Hydraulics Laboratory, Delft, the Netherlands, 10 pp.

de Vries, M. (1973), River-bed variations - aggradation and degradation, *Tech. Rep. 107*, Delft Hydraulics Laboratory, Delft, the Netherlands, 21 pp.

1305 Williams, R. D., R. Measures, D. M. Hicks, and J. Brasington (2016), Assessment of a numerical
1306 model to reproduce event-scale erosion and deposition distributions in a braided river, *Water*
1307 *Resour. Res.*, *52*(8), 6621–6642, doi:10.1002/2015WR018491.

1308 Woodhouse, M. J., A. R. Thornton, C. G. Johnson, B. P. Kokelaar, and J. M. N. T. Gray (2012),
1309 Segregation-induced fingering instabilities in granular free-surface flows, *J. Fluid Mech.*, *709*,
1310 543–580, doi:10.1017/jfm.2012.348.